

Reversible Discharge Products in Li–Air Batteries

Tong Liu, Siyuan Zhao, Qi Xiong, Jie Yu, Jian Wang, Gang Huang, Meng Ni,*
and Xinbo Zhang*

Lithium–air (Li–air) batteries stand out among the post-Li-ion batteries due to their high energy density, which has rapidly progressed in the past years. Regarding the fundamental mechanism of Li–air batteries that discharge products produced and decomposed during charging and recharging progress, the reversibility of products closely affects the battery performance. Along with the upsurge of the mainstream discharge products lithium peroxide, with devoted efforts to screening electrolytes, constructing high-efficiency cathodes, and optimizing anodes, much progress is made in the fundamental understanding and performance. However, the limited advancement is insufficient. In this case, the investigations of other discharge products, including lithium hydroxide, lithium superoxide, lithium oxide, and lithium carbonate, emerge and bring breakthroughs for the Li–air battery technologies. To deepen the understanding of the electrochemical reactions and conversions of discharge products in the battery, recent advances in the various discharge products, mainly focusing on the growth and decomposition mechanisms and the determining factors are systematically reviewed. The perspectives for Li–air batteries on the fundamental development of discharge products and future applications are also provided.

1. Introduction

To solve the energy crisis and environmental pollution caused by the excessive combustion of fossil fuels, the extension of electric vehicles is a crucial way to realize the sustainable development of human society.^[1] However, the widely used power supply in electric vehicles is Li-ion batteries, whose low theoretical energy density restricts the travel range and further application of electric vehicles.^[2] To meet the increasing demand for energy storage and conversion systems in daily life, it is necessary to explore new power batteries with high energy density.^[3] Among the various post-Li-ion batteries, such as solid-state Li-ion batteries, Na-ion batteries, lithium–sulfur batteries, and so on, lithium–air (Li–air) batteries with the highest energy density and environmentally friendly are regarded as the promised substitution for dominant Li-ion batteries (Figure 1a).^[4] A typical Li–air battery consists of an air cathode that the active oxygen does not need storing inside the battery, a lithium metal anode with high

energy density, and electrolytes with high ionic conductivity, operating via the simple redox reaction of $2\text{Li} + \text{O}_2 \leftrightarrow \text{Li}_2\text{O}_2$, 2.96 V versus Li/Li⁺ (Figure 1b).^[5] The unique reaction gives Li–air batteries an ultrahigh energy density of more than 3500 Wh kg^{−1}, far exceeding the state-of-the-art Li-ion batteries and other commercial batteries.^[6]

Unlike the lithium (de)insertion process in Li-ion batteries,^[7] the mechanism in Li–air batteries is electrocatalytic oxygen reduction/evolution reactions (ORR/OER) at the cathode side.^[8] Catalytic products, which need storage space, are generated after discharging and decompose via electrochemical routes after charging.^[9] Thus, the formation and decomposition of discharge products directly determine the performance of the Li–air battery.^[10] The discharge products can be easily formed and oxidized if the cathodic catalysts have high catalytic reaction kinetics; in this case, the battery can display a higher energy efficiency, rate performance, and power density.^[11] The amount of discharge products is related to the battery capacity: the more, the better. Higher conductivity and tighter contact with cathodes make the discharge products transfer the electrons easily, thus delivering a lower overpotential of the battery. The highly reversible products, which formed and fully decomposed many times without destroying the cathode structure and

T. Liu, S. Zhao, J. Yu, M. Ni
Building Energy Research Group
Department of Building and Real Estate
The Hong Kong Polytechnic University
Hung Hom
Kowloon

Hong Kong 999077, P. R. China
E-mail: meng.ni@polyu.edu.hk

T. Liu
The Hong Kong Polytechnic University Shenzhen Research Institute
Shenzhen, Guangdong 518057, P. R. China

Q. Xiong, G. Huang, X. Zhang
State Key Laboratory of Rare Earth Resource Utilization
Changchun Institute of Applied Chemistry
Chinese Academy of Sciences
Changchun, Jilin 130022, P. R. China
E-mail: xbzhang@ciac.ac.cn

J. Wang
School of Energy and Environment
City University of Hong Kong
Tat Chee Avenue
Kowloon
Hong Kong 999077, P. R. China

 The ORCID identification number(s) for the author(s) of this article can be found under <https://doi.org/10.1002/adma.202208925>.

DOI: 10.1002/adma.202208925

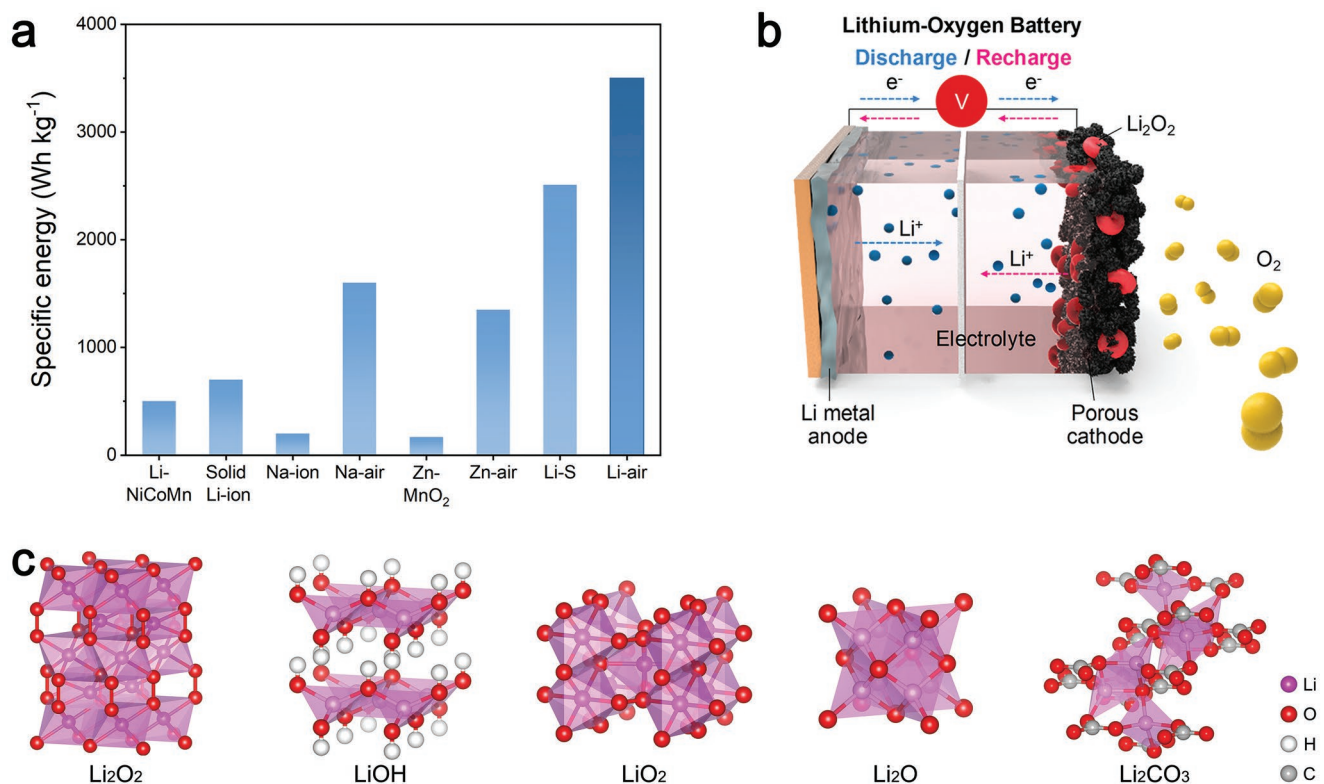


Figure 1. a) Comparison of the estimated practical specific energies for various rechargeable batteries. b) Schematic configuration of a Li–O₂ battery. b) Reproduced with permission.^[5] Copyright 2020, American Chemical Society. c) Crystalline structures of Li₂O₂, LiOH, LiO₂, Li₂O, and Li₂CO₃.

electrolyte oxidation, can result in long-term cycling stability of the batteries. Therefore, regulating discharge products is the key to realizing high-performance Li–air batteries.

In 1976, the Li–air battery prototype was first proposed in an aqueous system in which lithium reacts with H₂O to form LiOH.^[12] In 1996, the first nonaqueous lithium–oxygen (Li–O₂) battery that cycled via Li₂O₂ was reported.^[13] Because this battery concept was too advanced and had poor performance, the Li–air battery attracted attention until 2006.^[14] Bruce et al. revealed that Li₂O₂ is the predominant discharged product, which could decompose to release oxygen gas during charging. Since then, nonaqueous systems dominated the investigation of Li–O₂ batteries.^[15] Many efforts have been made to improve the proportion and reversibility of Li₂O₂ in the discharge products. Multiple cathodes with diverse characteristics, such as high catalytic activity, lots of hierarchical pores, self-supported structure, and integrated construction were designed.^[16] Various electrolyte systems with high ionic conductivity and stability for inhibiting side reactions caused by decomposition at high voltage were investigated.^[17] The lithium metal anode was protected from corrosion, dendrite, and volume change via in situ-formed solid electrolyte interphase film, alloyed anode, 3D framework, and so on.^[18] Indeed, these strategies could regulate Li₂O₂ and improve battery performance to a certain extent.^[19] Due to the insulating and oxidizing properties, typically discharge products Li₂O₂ in rechargeable nonaqueous Li–O₂ batteries^[15c] may trigger the nucleophilic attack on other components and sluggish reaction kinetics, inducing the decline of

performance and sometimes even premature death of batteries. Moreover, the road to commercialization of Li–O₂ batteries is still far away because it is tough to ensure the pure oxygen atmosphere working conditions; otherwise, it is necessary to develop advanced gas membranes, which only allow oxygen to transmit from the air.

To this end, investigating alternative reversible discharge products in the Li–air battery systems to improve the overall performance and reveal reaction mechanisms brought disruptive breakthroughs. For example, adding water and LiI for catalyzing LiOH,^[20] applying the Ir-based cathode for stabilizing the lithium superoxide (LiO₂),^[21] high-temperature for realizing reversible Li₂O,^[22] and cycling in CO₂ atmosphere to form Li₂CO₃.^[23] The crystalline structures of the products are shown in Figure 1c.^[24] However, to the best of our knowledge, few reviews have elaborated on the progress and fundamental science of the reversible discharge products in Li–air batteries.^[4b] In this review, we systematically summarized the current research progress of reversible discharge products in Li–air batteries to deepen the mechanistic understanding and promote future developments. We focused mainly on the formation and decomposition mechanisms for the products and the corresponding decisive factors, such as solvents, additives, adorability of intermediates, cathode catalytic activities, and operating conditions. We also presented the perspectives on the fundamental development regarding discharge products in the Li–air batteries and the challenges for their future practical application.

2. Li₂O₂

To exclude the influence of other impurity gases, most of the current Li–air batteries were discharged and charged in the pure oxygen atmosphere with a simpler kinetic model of Li₂O₂;^[25] thus, they could also be defined as Li–O₂ batteries. In the typical nonaqueous rechargeable Li–O₂ batteries, solid Li₂O₂ is considered as the primary products followed the basic reaction equations. In general, metallic lithium was oxidized to Li⁺ and released electron during discharging progress, the O₂ was reduced via ORR and obtained the electron from external circuit, then generated Li₂O₂ located at the cathode side. The charging progress was reverse, occurring OER, the Li₂O₂ was oxidized with oxygen evolution from the air cathode.^[26] The basic mechanism of charge–discharge processes is undoubted, and deepening the understanding of the fundamental properties of Li₂O₂ is also crucial for the ongoing development of Li–O₂ batteries.^[19]

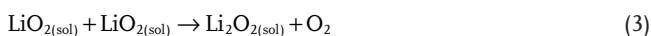
2.1. Li₂O₂ Formation

The detailed formation mechanisms of Li₂O₂ were classified into two categories, solution growth and surface growth.^[27] At the initial discharge, dissolved O₂ adsorbed on the cathode and then reduced to O₂[−] (Equation (1)), subsequently combined with Li⁺ in the electrolyte to generate LiO₂ intermediate (Equation (2)),^[28] which are the similarities between the two mechanisms^[29]



2.1.1. Solution Growth

In the electrolyte with high donor number (DN) which is beneficial to stronger Li⁺ solvation (Figure 2a), the formed LiO₂ will be dissolved into the solution via LiO₂* ⇌ Li⁺_(sol) + O₂[−]_(sol),^[30] subsequently disproportionating into Li₂O₂ and O₂ (Equation (3)) through the solution-growth pathway (Figure 2b)



In addition, some researchers proposed LiO₂ could chemically dissolve into Li⁺ and O₂[−] (Equation (4)). The soluble O₂[−] then combined Li⁺ to generate Li₂O₂ (Equation (5)), in which O₂[−] acts as a redox mediator on the growing Li₂O₂ toroid.^[29,31] Generally, the solution growth mechanism likely induces the growth of Li₂O₂ toroids/platelets with larger particle sizes than the surface growth mechanism resulting in conformal coated films,^[32] which was experimentally supported by Luntz et al.^[29] When added trace amounts of water in electrolyte, the products tended to grow via solution model with a large-size toroidal

Li₂O₂ and significant capacity improvement (Figure 2c). As the water can induce parasitic reactions during discharging, the solvents or additives with high DN and/or acceptor number (AN) that can promote the solution growth mechanism would be a better choice for improving capacity (Figure 2d).^[33]

In addition, by regulating the cathode surface, some catalysts also can promote the formation of Li₂O₂ via the solution pathway, even in a low-DN electrolyte. Xu et al. decorated the carbon nanotube (CNT) detects by coating the RuO₂ nanoparticles to alter its adsorption ability toward superoxide species LiO₂ and O₂[−].^[34] As shown in Figure 2e, the binding energies of LiO₂ (−1.72 eV) and O₂[−] (−0.82 eV) on the CNT surface are much higher than on RuO₂/CNT surface (0.21 eV, −0.13 eV). In this case, the superoxide species readily liberated from the RuO₂/CNT surface and diffused to the low-DN tetraethylene glycol dimethyl ether (TEGDME) electrolyte, biased to the solution growth of Li₂O₂. In contrast, the superoxide species are likely adsorbed on the pristine CNT surface, undergoing the surface growth route. As a result, micrometer-sized, flower-like Li₂O₂ generated on RuO₂/CNT, while conformal Li₂O₂ thin films deposited on pristine CNT surfaces. By reducing the adsorption energy of the cathode to the intermediates, the battery can realize toroid-like Li₂O₂ in the low-DN solvents via the solution growth pathway.^[33] Furthermore, the facet engineering of the cathode also can regulate the formation of the Li₂O₂ product. Yao et al. synthesized two kinds of β-MnO₂ crystals with (111) or (100) dominated facets.^[35] When adopted in Li–O₂ batteries, the (111) facets promoted the toroidal Li₂O₂ following solution routes, while (100) facets facilitated the thin-film Li₂O₂ through surface routes (Figure 2f).

2.1.2. Surface Growth

In the low-DN solvents, the formed LiO₂ is more easily adsorbed on the cathode surface (identified by *). It is prone to evolve into Li₂O₂ formation through electrochemical reduction (Equation (6)) or disproportionation (Equation (7)) via a surface-growth pathway (Figure 2a)^[36]



By conducting density functional theory (DFT) to calculate the relative energy changes in dimethyl sulfoxide (DMSO) and dimethyl ether (DME) electrolytes, as shown in Figure 3a, Kang et al. considered electrochemical reduction (Equation (6)) is more thermodynamically and kinetically favorable than disproportionation (Equation (7)).^[37] Shao-Horn et al. experimentally confirmed that surface-mediated O₂ reduction is related to the overpotential, based on electrochemical quartz crystal microbalance (EQCM) results.^[32] Along with the overpotential increases (below 2.5 V vs Li⁺/Li), soluble LiO₂ intermediates decrease, and thin conformal Li₂O₂ coatings form via the surface-mediated pathway (Figure 3b).

Besides the solubility of LiO₂ in electrolytes affects the Li₂O₂ growth routes through the surface or solution pathway,^[30] other studies have also tried to complement the formation

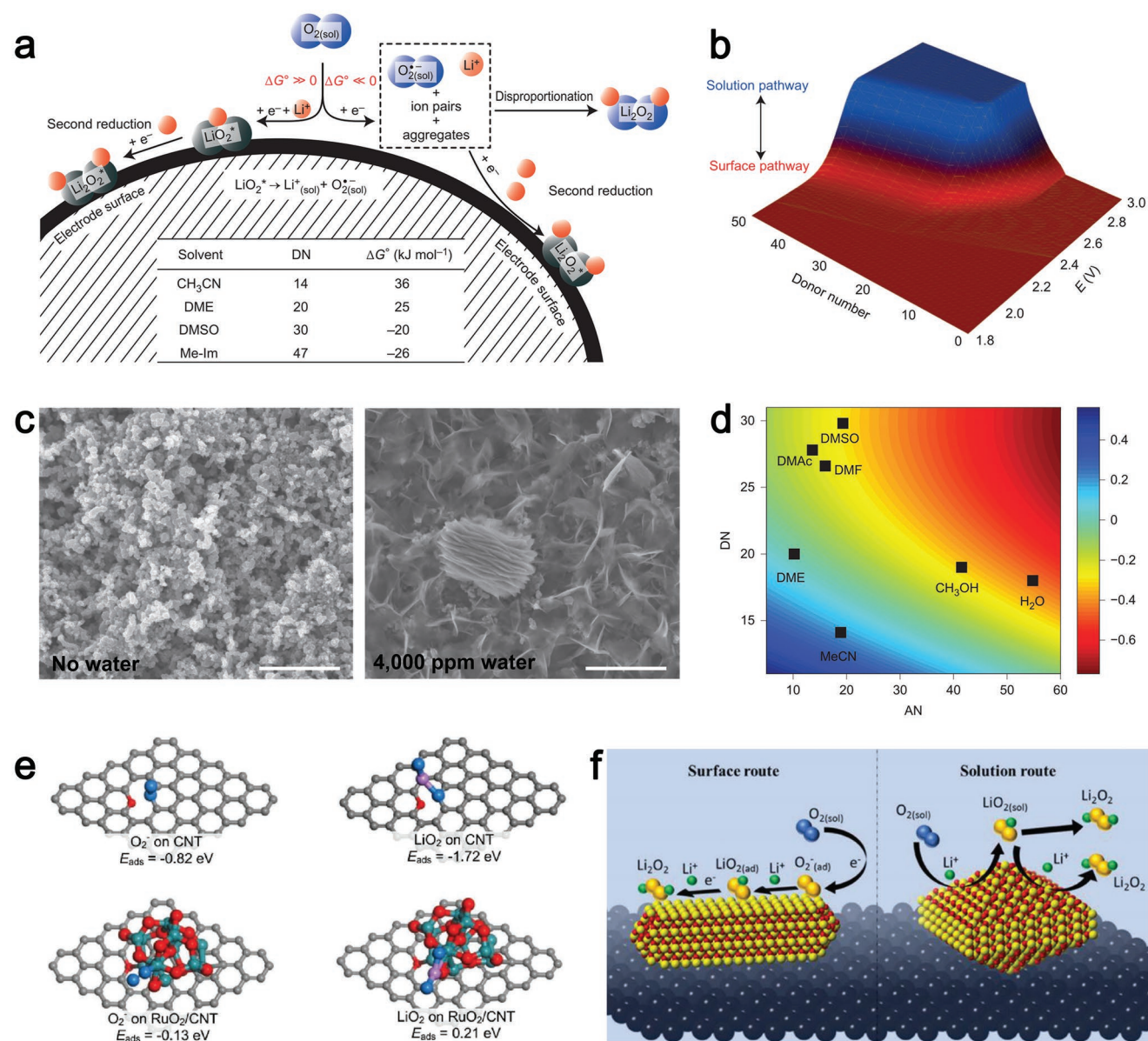


Figure 2. Solution growth of Li_2O_2 . a) High DN of solvents promote the Li_2O_2 growth via solution pathway, and b) a schematic shows the dominant pathway as a function of DN and discharged potential. a,b) Reproduced with permission.^[30] Copyright 2014, Springer Nature. c,d) High LiO_2^* solubility (such as adding water) boosts toroidal Li_2O_2 formation with a large size via solution growth: c) SEM images of discharge products Li_2O_2 (scale bars, 1 μm). d) The free energy of the solubility of LiO_2^* in different solvents as a function of the AN and DN. c,d) Reproduced with permission.^[29] Copyright 2015, Springer Nature. e) Cathode surface with low adsorption energy to the intermediates drives solution-mediated pathway: binding energies of O_2^- and LiO_2 on the double-defect CNT (top) and RuO_2/CNT (bottom). Reproduced with permission.^[34] Copyright 2016, Wiley-VCH. f) Cathode facets affect the Li_2O_2 growth pathway: (100)-dominated $\beta\text{-MnO}_2$ catalyzes Li_2O_2 formation following the surface route, (111)-dominated one following the solution route. Reproduced with permission.^[35] Copyright 2019, American Chemical Society.

mechanisms of Li_2O_2 . Chen et al. found the O_2 adsorbability on the cathode also determined the deposition types of Li_2O_2 based on a comparison of experimental and calculated results on different cathodes.^[38] Taking care of the limited electron transport on the electronically insulating Li_2O_2 , in the cathode neighborhood, Li_2O_2 tends to form into thin films via the surface growth route. Zhao et al. grew N, S co-doped CNTs on the 3D graphene (NS-CNTA/3DG), which successfully obtained an amorphous Li_2O_2 film products in $\text{Li}-\text{O}_2$ battery through the surface

route.^[39] The formation of amorphous Li_2O_2 is related to the high spatial confinement of doped elements, which benefits from the large surface area and stronger adsorption toward O_2 , Li, and LiO_2 (Figure 3c). This NS-CNTA/3DG cathode gave the battery a high capacity of 23 778 mAh g^{-1} and a long lifespan of 320 h (Figure 3d).

The current density also tuned the growth routes of Li_2O_2 products.^[40] Nazar's group found that the Li_2O_2 aggregated into toroidal nanocrystalline at low current density (Figure 3e).^[41]

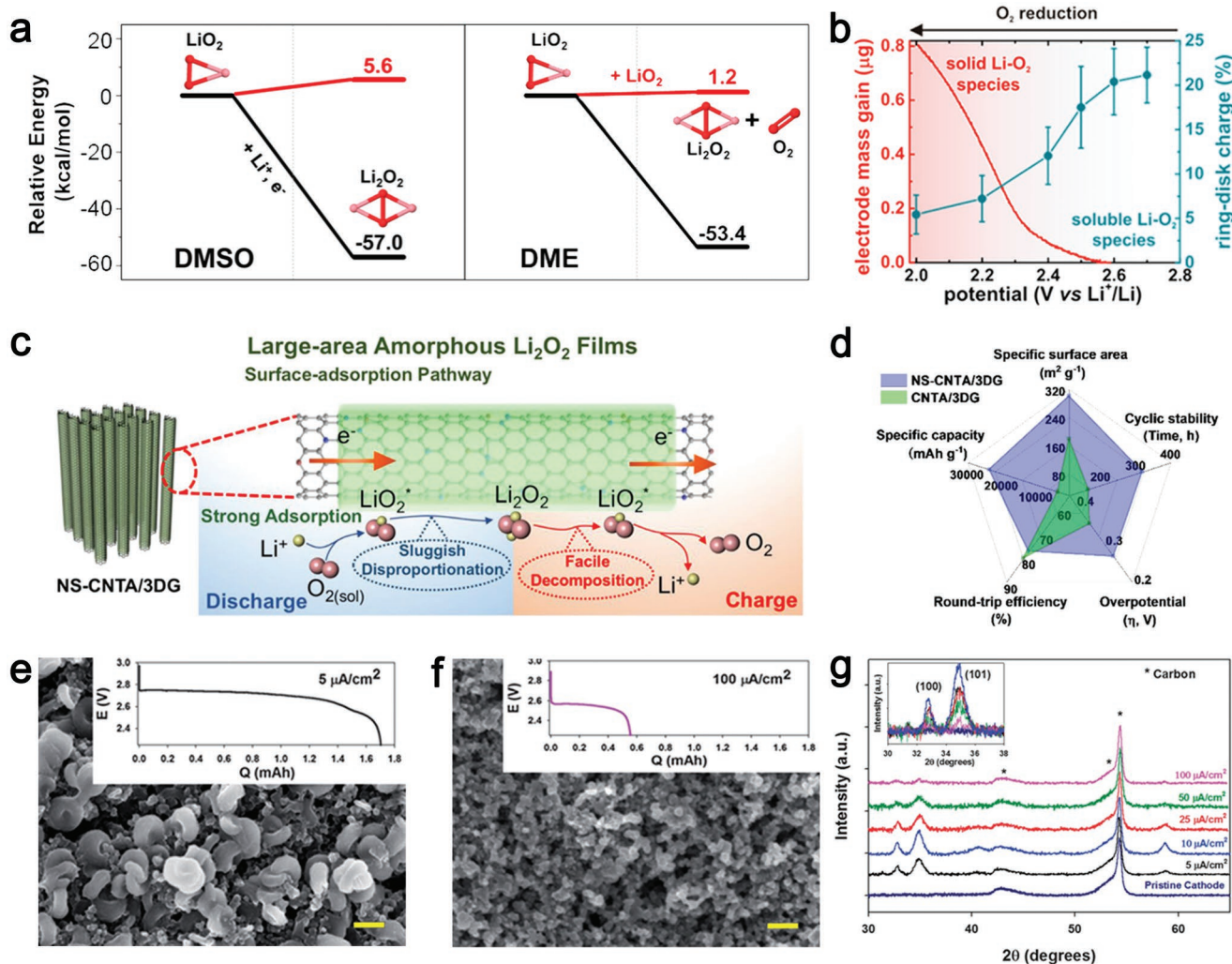


Figure 3. Surface growth of Li_2O_2 . a) Calculated DFT results show that LiO_2 is easily transferred to Li_2O_2 by the reduction reaction (black) pathway than the disproportionation reaction (red). Reproduced with permission.^[37] Copyright 2013, American Chemical Society. b) As the discharge potential decreases, soluble intermediates reduce, and Li_2O_2 dominant grows via surface pathway regardless of solvents. Reproduced with permission.^[32] Copyright 2016, American Chemical Society. c) The spatial confinement and stronger adsorption of NS-CNTA/3DG facilitates the Li_2O_2 growth through the surface route, d) along with improved battery performance. Reproduced with permission.^[39] Copyright 2022, Elsevier. e, f) High discharge current results in the Li_2O_2 formed through the surface model, verified by SEM images of cathode and after discharge at $5 \mu\text{A cm}^{-2}$ (e) and 100 mA cm^{-2} (f), and g) XRD results show that high current leads to a decrement of crystalline for discharge products. Reproduced with permission.^[41] Copyright 2013, The Royal Society of Chemistry.

They attributed to the weak binding of LiO_2 to the cathode surface and the slow electron transfer rate from surface, thus resulting in the LiO_2 disproportionation reaction through the solution pathway model. In contrast, at the higher discharge current, Li_2O_2 can readily form a thin film with less crystalline via the surface pathway (Figure 3f,g), which might be due to the newly formed LiO_2 on the cathode insufficiently dissolved in the electrolyte. In addition, it should be noted the discharge capacity and voltage decrease with the increase of current densities, which can be related to the morphological transition of discharge products. More amounts of toroid products could store in the porous cathode. By contrast, the thin-film products with smaller sizes likely cover the cathode surface to block the mass transfer channel,^[42] thus reducing the exposed active sites for ORRs and resulting in limited battery discharge capacity.

Moreover, unlike the toroidal Li_2O_2 with high crystalline, the thin-film Li_2O_2 with less crystalline is easier to be decomposed at lower charging potentials. Because their conformal contact to the cathode could supply more electron transfer, the oxidation of deficient Li_2O_2 needs less energy, enabling the decomposition of thin-film Li_2O_2 more easily.

In addition, the growth pathway of Li_2O_2 might affect by the temperature. Zhang et al. reported that at the low current density of 0.1 mA cm^{-2} , Li_2O_2 mainly formed through the solution route in the temperature range of -20 – $0 \text{ }^\circ\text{C}$, while through the surface route between 0 and $40 \text{ }^\circ\text{C}$.^[43] Furthermore, illumination also could influence product growth routes.^[44] Xu et al. reported that, without illumination, large-sized Li_2O_2 products generated randomly covered on the $\text{TiO}_2\text{-Fe}_2\text{O}_3$ photocathode via a solution-mediated growth pathway.^[45] While with

illumination, Li_2O_2 formed into thin-film morphology, which uniformly deposited. The difference may be attributed to, under illumination, intermediate LiO_2 is generated faster and likely concentrated at the cathode surface, which then disproportionated or reduced to form the film-like Li_2O_2 . In short, the LiO_2 might be the decisive factor for the Li_2O_2 growth pathway, whose generation rate, diffusion rate, and duration strongly influence on the products.

2.2. Li_2O_2 Oxidation

As the calculated density of states (DOS) shows (Figure 4a), pure Li_2O_2 present insulating performance with a large band gap of 4.91 eV.^[46] Undoubtedly, the insulating feature will limit electron mobility in pure Li_2O_2 and electron transport between the Li_2O_2 products and conductive cathode substrates, leading to the $\text{Li}-\text{O}_2$ batteries with poor rate capability and large polarization.^[47] For improving the $\text{Li}-\text{O}_2$ batteries' energy efficiency and cycling performance, it is significant to study Li_2O_2 oxidation during the charging progress.

Typically, the Li_2O_2 is oxidated from its surface, and the surface structure affects the decomposition progress. Mo et al. compared the desorption barriers and reaction path on different surfaces of Li_2O_2 using first-principles calculations.^[48] For all the calculated surfaces, the lithium peroxide first decomposed from Li atoms removal to form the superoxide intermediate, which was consistent with the experimental finding that LiO_2 was intermediate in $\text{Li}-\text{O}_2$ batteries.^[49] It is noteworthy that superoxide possesses the highest oxygen activity in the decomposition path and that is why the organic electrolytes would experience decompose in the $\text{Li}-\text{O}_2$ batteries.^[50] The followed oxygen evolution steps' energy barriers are remarkably higher than those of Li desorption along the decomposition path, demonstrating that the high overpotential and low charging rate of $\text{Li}-\text{O}_2$ batteries is probably resulting from the sluggish kinetics of OER.

Theoretically, pure Li_2O_2 is hardly oxidated due to its insulating nature, resulting in slow OER kinetics and high battery overpotential.^[27] Practically, the discharge products of Li_2O_2 in $\text{Li}-\text{O}_2$ batteries could be defected via chemistry engineering.^[51] The defects in Li_2O_2 can regulate its electronic conductivity and thus decrease the charging overpotential of the $\text{Li}-\text{O}_2$ batteries. By tailoring catalysts and electrolyte additives, they could also induce defects in Li_2O_2 , like Li vacancies ($\text{Li}_{2-x}\text{O}_2$), doped Li_2O_2 , amorphous structure, and others.^[47,52]

As shown in Figure 4a, Hummelshøj et al. used DFT calculations to compare the DOS for the pure Li_2O_2 and Li_2O_2 with Li vacancies.^[46] There are holes in the valence band and the Fermi level is shifting to valence bands, indicating that the $\text{Li}_{2-x}\text{O}_2$ presents electronic conductivity. Guo's group grew ZnO nanoparticles on vertically aligned CNTs (ZnO/VACNTs),^[53] generating the $\text{Li}_{2-x}\text{O}_2$ (mixture of LiO_2 , Li_3O_4 , and Li_2O_2) discharge products in $\text{Li}-\text{O}_2$ batteries, supported by the characterizations of transmission electron microscope (TEM) images (Figure 4b) and electron energy-loss spectroscopy (EELS) spectra. Along with the lithium vacancies introduced to the discharge product, the battery with ZnO/VACNTs cathode displayed a 1.5 times improvement of capacity and 0.45 V decrease of overpotential,

compared with pristine VACNTs (Figure 4c). Later, they coated semiconducting n-type Si on the CNTs,^[54] inducing the nano-sized Li_2O_2 with plenty of lithium vacancies, thus energy efficiency of the battery approaching 80%. Defective Li_2O_2 formed on semiconductors illustrates that cathode architecture plays a key role in the discharge products and thus affects the battery performance.

Doping heteroatoms in the Li_2O_2 could effectively improve its electronic conductivity by modulating the density and mobility of charge carriers. Timoshevskii et al. substituted 1.6% Li atoms with Si in the simulated Li_2O_2 electronic structure.^[55] As shown in DOS for Si-doped Li_2O_2 (Figure 4d), there are some conducting impurity states in the band gap of Li_2O_2 . Compared to the stoichiometric Li_2O_2 , the improved electronic mobility attributed to the antibonding orbitals of the oxygen pairs. Similarly, Zhao et al. demonstrated that adding carbon to Li_2O_2 could induce hole states in Li_2O_2 because of electron transfer from antibonding O–O p-orbitals to carbon.^[56] For the doping anions, Gerbig et al. indicated that the doped Cl⁻ can serve as a donor dopant to improve the ionic conductivity of Li_2O_2 via the experimental tests.^[57] Matsuda et al. revealed ≈ 5 mol% Cl could be incorporated into the Li_2O_2 products with the addition of LiCl into the electrolyte.^[58] The conductive atomic force microscopy was conducted to measure the electric conductivity of discharge products. As shown in Figure 4e, the detecting current value of Cl– Li_2O_2 is greater than 20 nA, while that of pristine Li_2O_2 is less than 20 pA. The higher electric conductivity aroused from Cl incorporation is beneficial to improving the energy capacity of $\text{Li}-\text{O}_2$ batteries. Regrettably, Cortes et al. carried out first-principles calculations and proposed that Cl doping cannot increase the electronic conductivity; because it did not promote the formation of metallic states or extra polarons on the Li_2O_2 .^[59] Undoubtedly, more experimental and simulation studies are needed to resolve this contradiction. Metal cations also can dope into the Li_2O_2 to modulate its physicochemical properties. Compared to the Na^+ , K^+ , the addition of Mg^{2+} , Ca^{2+} , and Ba^{2+} with larger sizes could apparently reduce the charge overpotential of the $\text{Li}-\text{O}_2$ batteries. Especially, the Ba^{2+} reached a Coulombic efficiency of 70%.^[60] The improvement may originate from the Ba^{2+} incorporated into Li_2O_2 deposits. The calculated model suggested that doping transition metals such as Co and Ni could improve charge transport in Li_2O_2 deposits by shifting the balance of Li^+ vacancies and hole polarons, resulting in low charge overpotentials even at high current densities.^[61]

Siegel's group compared the amorphous Li_2O_2 with crystalline Li_2O_2 using first-principles calculations.^[62] Although their band gaps and equilibrium electrochemical potentials are similar, demonstrating they are both wide-bandgap insulators. The amorphous Li_2O_2 displayed higher mobility and concentration of Li^+ vacancies, leading to a notable increase in ionic conductivity of 2×10^{-7} S cm^{-1} (Figure 4f) and a slight growth in electronic conductivity of 2×10^{-16} S cm^{-1} than crystalline Li_2O_2 . Peng et al. synthesized amorphous Li_2O_2 by a disproportionation reaction in acetonitrile solution and measured its ionic and electronic conductivities of 7.10×10^{-8} and 5.02×10^{-9} S cm^{-1} .^[63] The improved charge-transport properties of amorphous Li_2O_2 originate from the enhanced Li^+ mobility and O_2^- concentration, resulting in a lower charging potential (Figure 4g)

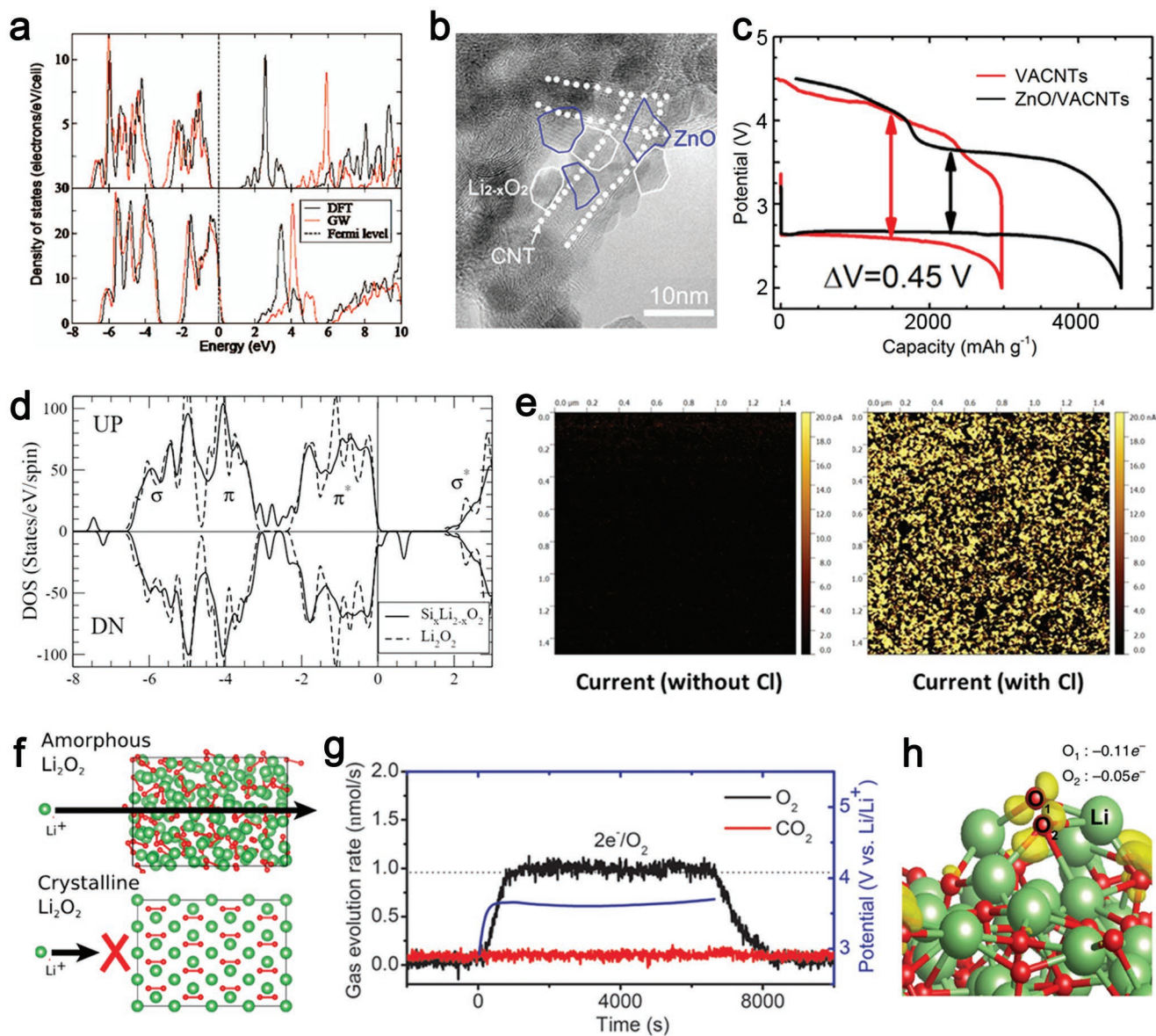


Figure 4. Li_2O_2 oxidation. a) Calculated DOS for pure Li_2O_2 (up) and Li_2O_2 with 1/16 vacancies (down), indicating the Li_2O_2 with Li vacancies present electronic conductivity, which is facile to the Li_2O_2 oxidation. Reproduced with permission.^[46] Copyright 2010, AIP Publishing. b) $\text{Li}_{2-x}\text{O}_2$ discharge products generated on the ZnO/VACNTs cathode, c) the Li–O₂ batteries with lower overpotential of 0.45 V. b, c) Reproduced with permission.^[53] Copyright 2016, Elsevier. d) Si-doped Li_2O_2 shows improved electronic mobility than undoped Li_2O_2 . Reproduced with permission.^[55] Copyright 2013, AIP Publishing. e) In the presence of 20×10^{-3} M LiCl, the discharge products exhibit higher electric conductivity. Reproduced with permission.^[58] Copyright 2016, American Chemical Society. f) Amorphous Li_2O_2 with much higher ionic conductivity than the crystalline phase. Reproduced with permission.^[62] Copyright 2014, American Chemical Society. g) The low overpotential of amorphous Li_2O_2 exemplifies the higher electron and ionic conductivity. Reproduced with permission.^[63] Copyright 2016, Wiley-VCH. h) The amorphous surface of Li_2O_2 has a weaker binding of LiO_2^* , beneficial to the desorption of intermediates and the decomposition of products. Reproduced with permission.^[65] Copyright 2018, Springer Nature.

compared with the crystalline phase. Based on the calculated and experimental results, it can be concluded that the products' crystallinity is related to the oxidation progress. That is, low crystallinity is facile to charging, which is also supported by Byon et al. They demonstrated that when CNTs surfaces were decoupled with oxygen functional groups or defective edges, the amorphous Li_2O_2 were formed, which was facilely decomposed in the subsequent charging progress.^[64] To further promote the decomposition of amorphous Li_2O_2 at low overpotential, it is

needed to increase the surface area of Li_2O_2 . Thus, they adopted a mesoporous carbon (CMK-3) as the cathode and successfully received 1D amorphous Li_2O_2 products in Li–O₂ batteries, leading to a high round-trip efficiency of 80%.^[65] The lower overpotential of OER and ORR in amorphous Li_2O_2 than the crystalline Li_2O_2 could be further evidenced by the DFT results that the disordered atoms on the surface caused the weaker binding to LiO_2 (Figure 4h). The amorphous Li_2O_2 was also observed on the noble metal surface with high binding energy

with LiO₂ that quickly nucleated on its surface and reduced to form the amorphous Li₂O₂ via surface route.^[66] Besides the cathode surface properties, the electrolyte solutions^[32,38] and the discharging current densities^[41] also affect the crystallinity of discharge products in Li–O₂ batteries as mentioned before, thus determining the charging progress.

3. LiOH

In the initial stage of Li–air batteries, LiOH (3.32 V vs Li/Li⁺) was regarded as the side product and averted as much as possible to reduce the cumulative negative impacts.^[67] Kwabi et al. revealed that flake-like LiOH gradually augmented along Li₂O₂ particles exposed to DMSO-based electrolyte, caused by the chemical reaction of electrolyte with Li₂O₂ and superoxide species.^[68] Unlike the rate-limiting step for the chemical release of O₂ molecules in the decomposition of Li₂O₂, the LiOH and Li₂CO₃ are electrochemical extraction of Li⁺.^[69]

3.1. LiI Promoted LiOH

As the OH[−] in LiOH is inert to the redox reaction, it needs to overcome a high energy barrier for Li desorption to generate a Li-deficient surface. Thus, incorporating a redox mediator could compensate for the electron loss in the decomposition of LiOH, improving the kinetics. Kwak et al. found that LiOH majorly precipitated rather than Li₂O₂ when added high concentrations of LiI to TEGDME electrolytes.^[70] LiOH-induced battery capacity decrease was regarded as a drawback to the additive LiI. They attributed the formation of LiOH to the decomposition of solvent, which was later verified by Qiao et al.^[71] that LiI could promote the nucleophilic reactions of discharge intermediate toward electrolytes. Soon after, Grey group added 0.05 M LiI into the Li–O₂ batteries composed of graphene oxide cathode and 0.25 M LiTFSI/DME electrolyte.^[20] In this case, the Li–O₂ batteries realized operation via the reversible growth and decomposition of crystalline LiOH (Figure 5a), demonstrating enhanced specific capacities at various current densities, a superior energy efficiency of 93.2% with a low overpotential of 0.2 V at 0.02 mA cm^{−2} (Figure 5b), a high discharge current up to 5 Ag^{−1} (equivalent to 0.1 mA cm^{−2}), and ultralong cycle life. The additive LiI served as the redox mediator to guide the battery's working voltage and cycling stability; it coupled with additive H₂O to induce the formation of LiOH as discharge products, increasing the battery capacity. Based on the NMR measurements with isotopic labeling, the proton in LiOH preferentially supplied from added water rather than DME decomposition. Regrettably, the desirable features aroused from LiOH were hard to reproduce even in the same electrolyte but changing the cathode. Later, they found that the LiOH only could be formed in the presence of both LiI and water, whereas Li₂O₂ was generated with either.^[72] The product types can be controlled by adjusting the water content in LiI-additive Li–O₂ battery. The dominant Li₂O₂ changed to LiOH with an appropriate amount of water in the battery, then transformed to a mixture of peroxides and hydroxides along with increased water, consistent with Shao-Horn et al.'s

study.^[73] Via the NMR spectroscopy, they demonstrated again that the proton source for LiOH was water rather than the decomposition of ether electrolyte.^[72] McCloskey et al. reported the same conclusions based on the products reverted from LiOH to Li₂O₂ after the additive H₂O entirely consumed, meaning without water, only LiI cannot promote the formation of LiOH.^[74] Besides the products of LiOH, Zhu et al. found that LiOOH·H₂O formed along with LiOH in the water-contaminated Li–O₂ battery with additive LiI redox (Figure 5c).^[75] DFT results demonstrated that the LiOOH·H₂O possessed similar structure to LiOH·H₂O, leading to the similar stability. Compared with Li₂O₂ and LiOH, LiOOH·H₂O displayed faster kinetics in the oxidation progress of I[−] to I₃[−], enabling a lower overpotential upon charging. In addition, they also proposed a panoramic mechanism of discharging/charging progress with different H⁺ concentrations.

It is noteworthy that the ambiguities exist in the LiI's effects on product decomposition during charging progress due to the complexity of the systems in that Li–air batteries contain water and polyvalent iodine.^[76] The additive LiI will undergo a mutual conversion of iodide/triiodide/iodine (I[−]/I₃[−]/I₂) redox, in which the I[−] can be oxidated to I₃[−] and I₃[−] oxidated to I₂ upon charging.^[76a,77] Liu et al. confirmed the LiOH can be chemically oxidated by I₃[−] to generate O₂ and H₂O in the DME electrolyte via the reaction of 4LiOH + 2I₃[−] → 4Li + 6I[−] + 2H₂O + O₂.^[20] However, in the presence of LiI and water, Burke et al.^[74] found that LiOH cannot be oxidized to form O₂ but irreversibly formed lithium iodate (LiIO₃) via 3I₂ + 6LiOH → LiIO₃ + 5LiI + 3H₂O, while the O₂ generated from Li₂O₂ based on the isotopic labeling results. The concentrations of LiI and H₂O significantly affected the products' decomposition. Qiao et al. also reported that, a large amount of LiI could promote the LiOH formation during discharged progress of LiI-added Li–O₂ batteries. However, in charging progress in the TEGDME solution, LiOH refused to be oxidized by the formed I₃[−] and I₂, while I₃[−] could decompose Li₂O₂ (Figure 5d).^[71] The difference among the reports of LiI-added Li–O₂ batteries might be attributed to the system diversity, in which the electrolyte is crucial for the electrochemical progress.^[20] The TEGDME solvent has a higher viscous and a lower donor number (DN) of 16.6 kcal mol^{−1} than DME (DN = 20 kcal mol^{−1}).^[78] Thus, Shao-Horn et al. systematically investigated the additive LiI toward catalyzing the decomposition of LiOH and Li₂O₂ in different solvents.^[76a] As shown in Figure 5e, the potential of I₃[−]/I[−] redox couple shifts toward higher potential while that of I₂/I₃[−] experiences no obvious change in the solvents with higher acceptor number, DN, and dielectric constant, proving stronger solvation of I[−] ions. After adding commercial LiOH and standing for a while, the I₃[−] was fully consumed in the solvents with strong solvation ability (DMA, DMSO, and Me-Im), while there is no reaction in weak ones (G4, DME, and pyridine), suggesting the reaction of I₃[−] oxidizing LiOH is solvent dependent (Figure 5f). Via I₃[−] + 2LiOH → 2I[−] + 2Li⁺ + H₂O + IO[−], the formed IO[−] further disproportionated to LiIO₃ or decomposed the solvent molecules. And the LiIO₃ could further be reduced to form LiOH via a six-electron reaction of LiIO₃ + 3H₂O + 6Li⁺ + 6e[−] → LiI + 6LiOH.^[76b] For Li₂O₂, I₃[−] could effectively oxidize it to generate O₂ in the stronger solvents, whereas more oxidizing I₂ with higher potential is required in weaker solvents.

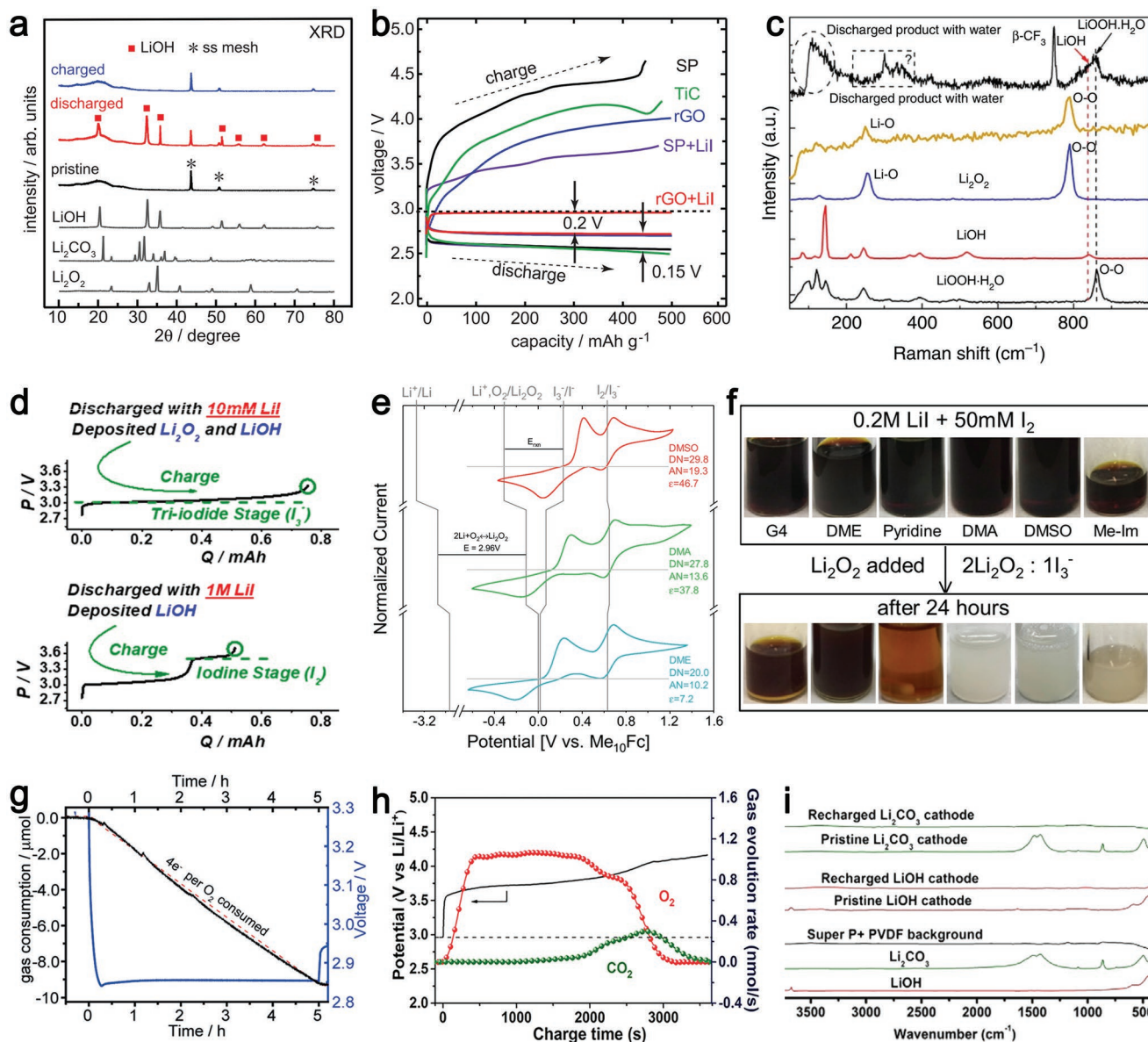


Figure 5. LiOH. a) Crystalline LiOH formed and decomposed in the Li–O₂ battery with rGO cathode and LiI additive, b) and it displays a low overpotential of 0.2 V. a,b) Reproduced with permission.^[20] Copyright 2015, AAAS. c) LiOOH·H₂O generated along with LiOH and Li₂O₂ in the water-added Li–O₂ battery. Reproduced with permission.^[75] Copyright 2017, Springer Nature. d) I₃⁻ hardly oxidizes LiOH but could decompose Li₂O₂. Reproduced with permission.^[71] Copyright 2017, American Chemical Society. e) Solvents determine the redox potentials of I₃⁻/I⁻ and oxidizing power of I₃⁻/I⁻ toward Li₂O₂ in different solvents. e,f) Reproduced with permission.^[76] Copyright 2019, Elsevier. g) With the addition of water, Ru-catalyzed battery forms LiOH via a 4e⁻ ORR. Reproduced with permission.^[82] Copyright 2017, Wiley-VCH. h) Adding H₂O boosts the formation of LiOH, which cannot contribute to O₂ evolution during recharge, confirmed by DEMS detecting less oxygen release. Reproduced with permission.^[83] Copyright 2018, American Chemical Society. i) DBDMB has the catalytic activity toward the oxidation of Li₂CO₃ and LiOH. Reproduced with permission.^[84] Copyright 2020, Wiley-VCH.

Investigations of soluble redox mediators in Li–air batteries have made considerable progress. The redox mediators, such as LiI, TTF (tetrathiafulvalene), FePc (iron phthalocyanine), DMPZ (5,10-dimethylphenazine), could significantly accelerate the transformation of discharge products and lower the battery overpotential.^[79] However, it still needs advanced in situ techniques for real-time monitoring of the electrochemical progress of the battery, which could provide more information during the dynamic reactions and gain more insights into the mechanisms.

3.2. Water Catalysis LiOH

The addition of water can not only increase the battery capacity^[80] but also promote the formation of LiOH products in Li–O₂ batteries. By adding a trace amount of water, Li et al. found the discharge product can convert Li₂O₂ to LiOH by adjusting the battery discharge depth.^[81] A low voltage gap (0.32 V) and superior cycling stability (200 cycles, 800 h) were observed, in which the Li–O₂ battery constructed by Ru/MnO₂/SP cathode and LiFePO₄ anode, and 0.5 M LiClO₄ and

120 ppm H₂O in DMSO as the electrolyte. Grey et al. added 50 000 ppm water to the DMSO electrolyte, and thus the Ru/SP-catalyzed battery's discharge products were changed from Li₂O₂ to LiOH.^[82] Operando pressure measurement showed the LiOH formation involved four electrons with the overall reaction of O₂ + 4e⁻ + 4Li⁺ + 2H₂O → 4LiOH (Figure 5g). In the charging progress, LiOH decomposed with very little oxygen evolution due to the generated hydroxyl species chemically reacting with DMSO to form DMSO₂ rather than O₂. Therefore, a stable electrolyte that could prevent the reaction with LiOH during charging is highly desired to realize the high reversibility of LiOH.^[76a] In addition, Peng et al. also verified that the decomposition of LiOH did not contribute to oxygen evolution during recharge progress as the added H₂O intruded the decreased quantity of O₂ evolved.^[83] As shown in Figure 5h, differential electrochemical mass spectrometry (DEMS) data indicated that water-induced LiOH could alleviate O₂ and CO₂ release, meaning water could slightly destroy the battery reversibility. By in situ spectroscopic analysis and isotopic characterization, the lower charging polarization of H₂O-involved Li–O₂ battery was attributed to the higher conductivity of LiOH (ionic conductivity: 1.99 × 10⁻⁸ S cm⁻¹, and electronic conductivity: 7.13 × 10⁻¹² S cm⁻¹) than that of insulating Li₂O₂. Zhang et al. introduced a new redox mediator of 2,5-di-*tert*-butyl-1,4-dimethoxybenzene (DBDMB), which can facilitate the Li₂O₂ decomposition and even oxidize the LiOH and Li₂CO₃ at a relatively low overpotential (Figure 5i).^[84] The DBDMB may be an effective additive for increasing the Li–O₂ battery performance that operates via LiOH. Meanwhile, many challenges, including practical electrochemical behavior and redox mechanisms of LiOH products, need to be addressed for such additives.

3.3. Catalysts Promote LiOH Formation

Motivated by the excellent performance and high stability of LiOH, it attracted more attention as a reversible discharge product in Li–O₂ batteries.^[85] By comparing the different catalysts' performance in battery, Zhou et al. found catalysts were highly related to the formation/decomposition of LiOH.^[81] Song et al. synthesized a Mn-MOF-74 nanoparticles grown on CNTs (Mn-MOF-74@CNTs) catalyst which could change the product from Li₂O₂ to LiOH when operating in a humid atmosphere (≥200 ppm moisture).^[86] Compared with the battery with Li₂O₂ products, the MOF-74@CNTs-based battery cycled on LiOH displayed fewer side reactions and much-improved performance, which was attributed to less reactivity of LiOH than Li₂O₂. A mechanism was proposed that LiOH formed by chemical conversion (Li₂O₂ + H₂O → 2LiOH + ½ O₂) rather than a 4e⁻/O₂ electrocatalytic ORR, whose calculated standard Gibbs free energy was -75.0 kJ mol⁻¹. The Mn²⁺/Mn³⁺ metal centers in Mn-MOF-74@CNTs had high catalytic activity toward the decomposition of intermediate H₂O₂, which remarkably facilitated the chemical reaction. On the contrary, Grey et al. prepared Co₃O₄ catalysts with the flake structure to boost the electrochemical conversion of LiOH in the presence of water.^[87] In the discharging process, via a 4e⁻/O₂ process, Co₃O₄ could facilitate the formation of LiOH flakes with some side products, such as organics and carbonates; in addition, its surface formed

a reconstructed amorphous CoO_x(OH)_y layer. When charging, LiOH was oxidized at 3.9 V and released O₂ gas, followed by the decomposition of surface organics, and finally carbonates over 4.3 V. After charging to 4.5 V, the amorphous layer disappeared and resumed to Co₃O₄. The surface reconstruction of catalysts might be a potential strategy for catalyzing LiOH operating in Li–O₂ batteries, whose dynamic properties need more exploration.^[88] In addition to metal compound catalysts, Amine et al. demonstrated that the soluble metal cation additive, sodium ions, can boost the formation of reversible LiOH instead of Li₂O₂.^[79b] It was attributed to the added Na⁺ could alter the solvation environment and equilibrium in the electrolyte.

4. LiO₂

4.1. Exploration of LiO₂

LiO₂ (2.76 V vs Li/Li⁺) is usually considered as the reaction intermediate in Li–O₂ batteries, which would immediately evolve into lithium peroxide through electrochemical reduction or disproportionation reactions.^[30,89] Noteworthy, the LiO₂ with strong oxidizing property could react with various electrolytes and corrode the carbon electrodes.^[90] However, Lu and Shao-Horn believed that the low overpotentials in initially charging progress of Li–O₂ batteries were associated with the formed LiO₂-like species on Li₂O₂ particles.^[91] Curtiss and co-workers also detected the oxygen-rich LiO₂-like component and Li₂O₂ incorporated into the discharging products,^[92] in which the former products exhibited lower charging voltage (3.2–3.5 V) than the later one (≈4.2 V). To reveal the stability of LiO₂, they performed high-level quantum chemical calculations (G4MP2).^[93] The calculated activation barriers for oxygen evolution of large-sized LiO₂ clusters were higher than the dimer, confirming that the LiO₂ could survive in the discharge products. Later, they developed a mesoscale model for producing a microstructured LiO₂.^[94] The model predicted during discharging progress, the continued deposition of LiO₂ induced the large particles to grow faster and delayed the dissolution of the smaller ones. As a result, the LiO₂ tended to grow into large particles, and the small ones disappeared. They also studied the interfacial effects toward the disproportionation of LiO₂.^[95] With the protection of electrolyte, the LiO₂ component (Figure 6a) could be detected after resting for 70 h, while only 20 h in the vacuum without electrolyte (Figure 6b). Ab initio molecular dynamics (AIMD) simulations confirmed the amorphous LiO₂ slab had more stable interfacial energy when exposed to the electrolyte than vacuum. The combined experimental and theoretical studies indicated that the interface could slow the disproportionation process, and thus stabilizing the LiO₂.

Based on these investigations, LiO₂ could become the reversible discharge product generated in discharging and decomposed in the recharging progress of Li–O₂ batteries. The LiO₂ formed via a simplified route that O₂ reduced by e⁻ at the cathode surface and reacted with Li⁺ (Li⁺ + O₂ + e⁻ ⇌ LiO₂). Compared with the two-electron oxygen reaction of Li₂O₂, the LiO₂ based on one-electron demonstrated fast dynamics.^[51,96] The theoretical studies implied the oxygen evolution kinetics for LiO₂ decomposition were faster than Li₂O₂.^[97] In addition,

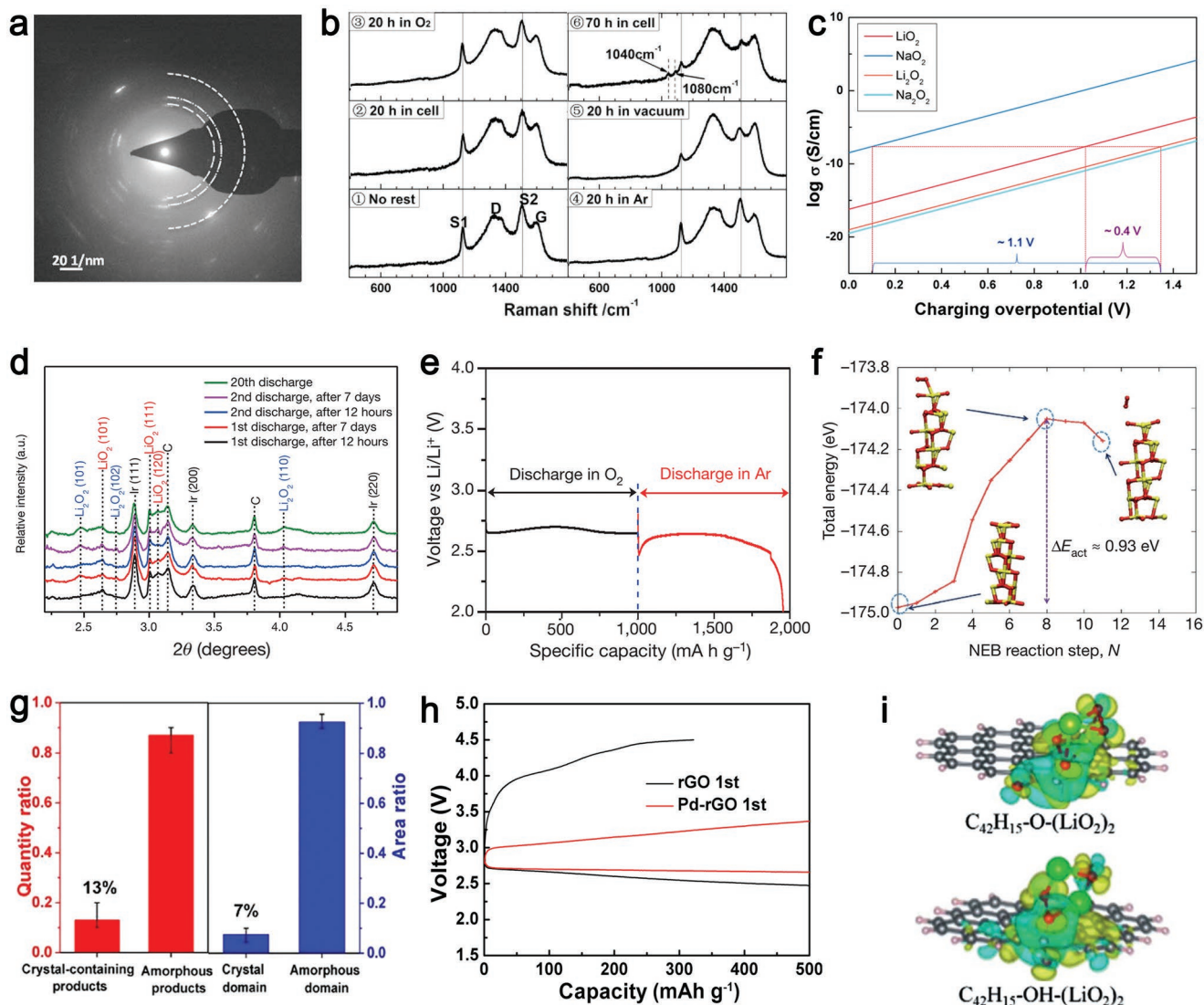


Figure 6. LiO₂. a) TEM image shows LiO₂ formed after discharging; b) LiO₂ could stabilize on the cathode surface for days. a, b) Reproduced with permission.^[95] Copyright 2015, American Chemical Society. c) LiO₂ has higher ionic conductivities. Reproduced with permission.^[97] Copyright 2015, American Chemical Society. d) LiO₂ can be stabilized on Ir-rGO cathode after discharge for days; e) LiO₂ products can converse into Li₂O₂ in the Ar and release another ≈96% capacity; f) DFT of oxygen desorption reveals the crystalline LiO₂ is thermally stable. d–f) Reproduced with permission.^[21] Copyright 2016, Springer Nature. g) Statistics from the cryo-TEM display that the discharge products are mainly amorphous phase. Reproduced with permission.^[99] Copyright 2022, American Chemical Society. h) Pd-rGO catalyzes the amorphous LiO₂ products in Li–O₂ battery, dramatically reducing the voltage gap to 0.3 V at 200 mA g^{−1}. Reproduced with permission.^[100] Copyright 2017, Elsevier. i) Charge density difference exhibits the electrons transfer to LiO₂, which may reduce its oxidizability. Reproduced with permission.^[103] Copyright 2022, The Royal Society of Chemistry.

LiO₂ exhibited much higher ionic conductivities (Figure 6c) and markedly low dissolution energy in electrolyte than Li₂O₂. Thus, forming the alternative LiO₂ during discharge rather than Li₂O₂ might be an available strategy to improve the performance of Li–O₂ batteries.

4.2. LiO₂ on Cathodes

Lu et al. obtained the stable crystalline LiO₂ which could be repeatedly formed and decomposed in the Li–O₂ batteries based on a suitable iridium–reduced graphene oxide (Ir–rGO) cathode.^[21] The DEMS and high-energy X-ray diffraction

(HE-XRD) results indicated the existence of the LiO₂ while there is no Li₂O₂ present when the battery shallow discharged (Figure 6d). As shown in Figure 6e, the Li–O₂ batteries with Ir–rGO cathode discharged to 1000 mAh g^{−1} capacity in O₂ could release another ≈96% capacity in Ar, while few gave for the rGO cathode. Based on the reaction of Li⁺ + e[−] + LiO₂ → Li₂O₂, the additional capacity was evidence of LiO₂ formation on the initial discharge, and the presence of LiO₂ could be attributed to the Ir–rGO cathode. This cathode with high ORR activity favored nucleation and growth of LiO₂, in which some crystalline faces of Ir₃Li intermetallic compound matched well with those of LiO₂. They also evaluated the kinetic stability of LiO₂ via computational studies. DFT calculation result for the desorption

barrier of O₂ leaving the crystalline LiO₂ products surface was higher than the amorphous one, indicating the former was thermally stable (Figure 6f). The AIMD results showed that the electrolyte which adsorbed on amorphous LiO₂ could suppress its disproportionation, thus increasing the lifetime of LiO₂ in a discharge product. The experimental and theoretical evidence confirmed that LiO₂ is stable in this Li–O₂ system, enabling a low charge potential of 3.2 V. Later, the LiO₂ products were successfully detected by aberration-corrected environmental TEM.^[98] Although the LiO₂ disproportionated into Li₂O₂ and O₂ after 100 s, it was evident that LiO₂ could be stable for a while and potentially be a rechargeable product. Recently, to exclude the effects of electron beam irradiation which may lead to crystallization of amorphous products, Gu et al. used cryogenic-TEM to study the toroidal discharge products in Li–O₂ batteries.^[99] The results revealed that the toroidal products were primarily composed of amorphous LiO₂ with a tiny amount of crystalline Li₂O₂ (Figure 6g). The amorphous LiO₂ was also obtained based on a 3D-architected Pd-rGO cathode, and the resultant battery displayed an ultralow overpotential of 0.3 V (Figure 6h).^[100] Besides the Ir₃Li intermetallic,^[21,101] Curtiss et al. recently synthesized IrLi nanoparticles and it enabled the formation of LiO₂ in Li–O₂ batteries.^[102] The DFT analysis illustrated the lattice matching of LiO₂ (111) with the (111) and (110) facets of IrLi; thus, the LiO₂ was favorable to grow on the IrLi surface. Sun et al. proposed a new sealed battery that cycled by interconversion of the reversible LiO₂ and Li₂O₂.^[103] The induced oxygenated group on reduced graphene oxide aerogel could stabilize the LiO₂, supported by DFT results of electrons transferred from graphene sheets to LiO₂, as shown in Figure 6i. This sealed battery exhibited a long cycling lifetime of 700 cycles at 0.6 mA cm^{−2}, presenting a new avenue for the reversible LiO₂ and Li₂O₂ in Li–O₂ batteries. It is noteworthy that besides the widely used Raman spectroscopy, DEMS, and electron diffraction to identify the presence of LiO₂, other characterization techniques and in situ tests should be employed to verify these discharge products, which are usually identified as intermedial, including EELS, X-ray absorption near edge structure, X-ray photoelectron spectroscopy, and EQCM.^[96,98]

5. Li₂O

Compared with Li₂O₂ and LiO₂, Li₂O (2.91 V vs Li/Li⁺) is more stable and does not react with organic solvents due to its poor oxidative nature.^[24b] However, the formation of Li₂O needs high energy to break the O–O bond of O₂ molecule,^[27] and to conquer the higher standard Gibbs reaction energy than Li₂O₂; thus, it is not thermodynamically and kinetically favored under ambient conditions (Figure 7a).^[22] In addition, Li₂O is insulting from both the bulk and surface, making it an inappropriate chemical reaction product of Li–O₂ batteries since the absence of facile pathways for electron transport might result in poor reversibility of the battery.^[104] As shown in Figure 7a, when the temperature increases to around 150 °C, the lithium reacts with oxygen and would like to thermodynamically form Li₂O rather than Li₂O₂. According to this, Nazar et al. demonstrated a Li–O₂ battery with an adjusted battery configuration, which can operate via four-electron transfer to form Li₂O at 150 °C. They

took the LiNO₃/KNO₃ eutectic molten salt as the electrolyte, Li_{1.5}Al_{0.5}Ge_{1.5}(PO₄)₃ as the protective membrane for Li anode, and the in situ formed Li_xNiO₂ as the bifunctional ORR/OER catalyst to boost the reversible O–O bond cleavage and O₂ evolution. Compared with the aprotic electrolyte (0.5 M LiTFSI/TEGDME) at 25 °C, the proposed high-temperature Li–O₂ batteries based on Li₂O products displayed a highly increased capacity of 11 mAh cm^{−2} with a low overpotential of 0.2 V (Figure 7b). The Raman spectra in Figure 7c showed the generation and removal of Li₂O on the Ni-based cathode, while the Li₂O₂ formed on the carbon cathode. Online mass spectrometry analysis manifested the charging progress of Ni-based composite cathode based on four-electron transfer from Li₂O with the electrochemical reaction of 2Li₂O → 4Li⁺ + O₂ + 4e[−]; by contrast, the carbon cathode based on 2e[−]/O₂ coupled with lots of parasitic reactions (Figure 7d). Benefiting from the excellent rechargeability of the cathode, the obtained battery displayed a stable cycling life of 150 times with a Coulombic efficiency of 100% (Figure 7e). In addition, along with the operating temperature increasing, the ratio of Li₂O in discharge products increased, attributed to the accelerated disproportionation from desorbed Li₂O₂ to Li₂O (Figure 7f). This work demonstrated that the elevated temperatures could facilitate the reversible conversion of Li₂O instead of Li₂O₂, and the obtained Li–O₂ batteries based on Li₂O possessed fast kinetics and impressive performance, which may inspire further research to verify its potential and practicality. In addition, similar to Li–O₂ batteries, a new rechargeable-battery chemistry based on lithium oxide growth was proposed.^[105] The battery operated at 150 °C through nitrate anion redox: 2Li + LiNO₃ → Li₂O + LiNO₂, in which molten LiNO₃/KNO₃ eutectic salt served as both active material and the electrolyte.

Before the above-mentioned sealed LiO₂/Li₂O₂ battery, Okuoka et al. reported a sealed battery that operated on the redox reaction between Li₂O and Li₂O₂ (2Li+Li₂O₂ ⇌ 2Li₂O).^[106] The Co-doped Li₂O cathode effectively accelerated the decomposition of Li₂O for converting it into Li₂O₂, exhibiting a reversible capacity of 190 mAh g^{−1}. Due to LiO₂ could deliver an additional capacity in the Ar atmosphere,^[21] as shown above in Figure 6e, Lu and colleagues further proposed a new battery that cycled between the condensed particles (Li₂O₂ + 2Li⁺ + 2e[−] = 2Li₂O, LiO₂ + 3Li⁺ + 3e[−] = 2Li₂O) without O₂ evolution (Figure 7g).^[107] The cathode composed of nanoporous Co₃O₄ and amorphous Li₂O delivered a low overpotential of 0.24 V and a high capacity of 587 mAh g^{−1}. Accompanied by a Li₄Ti₅O₁₂ anode that replaced the lithium metal, the battery in the sealed condition gave high safety, demonstrating better application potential than traditional Li–air batteries. Besides the cobalt-based catalyst, other catalysts also can be applied in this kind of sealed battery. For example, Zhou et al. employed a Li₂O-embedded Ir–rGO electrode for the sealed Li₂O/Li₂O₂ battery with no superoxide or oxygen evolution by the rationally controlled charge depth (Figure 7h).^[108] The formed intermetallic Li_{2−x}O₂–Ir compound on the cathode enabled the battery with an over 400 mAh g^{−1} capacity, 0.12 V overpotential, and 2000 stable cycles (Figure 7i). Recently, Kang and co-workers reported a molten nitrate salt-based sealed Li–O₂ batteries with the Fe₃O₄ as cathodes, which also could operate at 150 °C.^[109] Such kinds of sealed batteries based on reversible lithium oxygenates, although cannot strictly speaking lithium–air batteries, reveal high safety and good

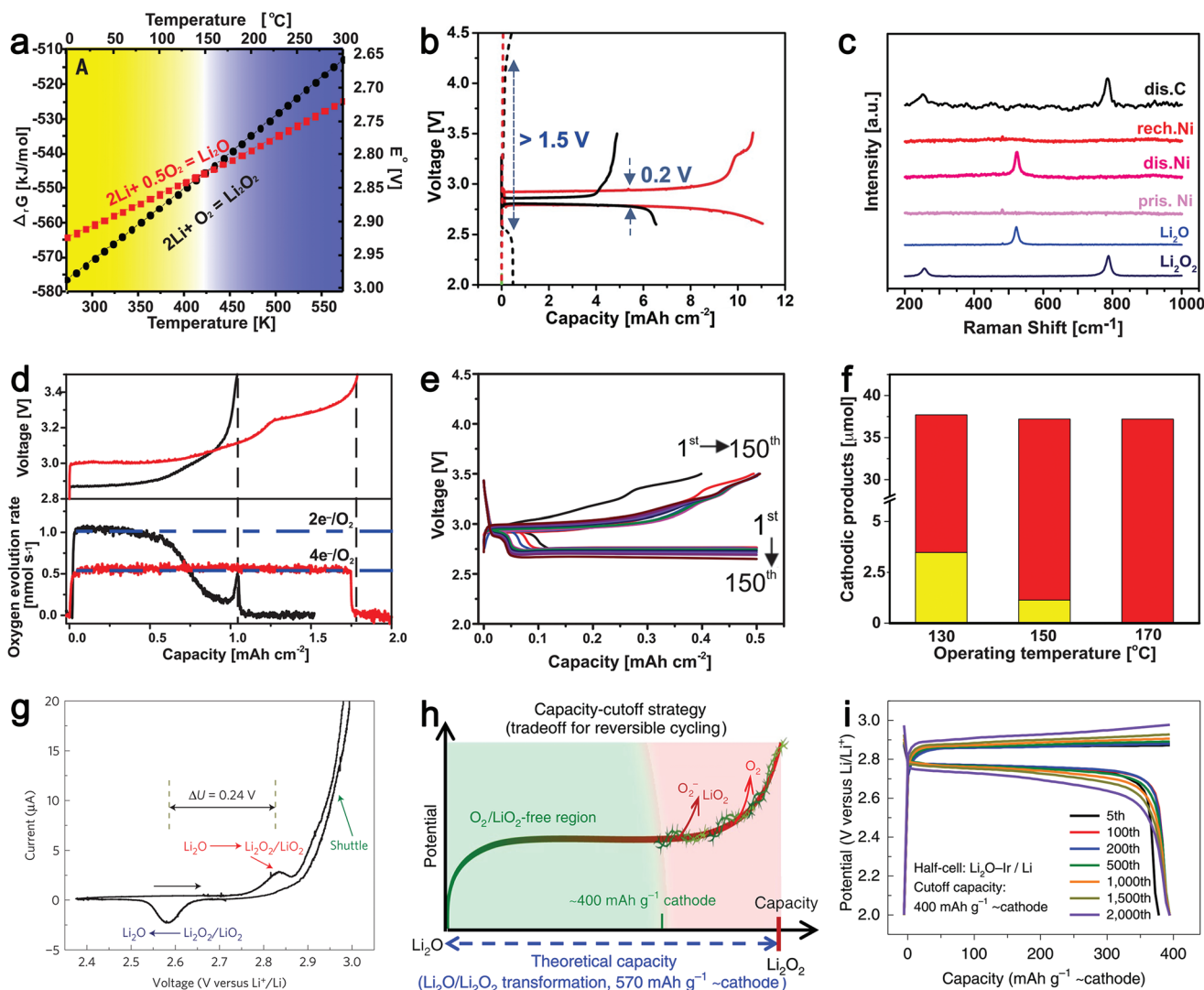


Figure 7. Li_2O . Li_2O formed under a high temperature: a) Gibbs reaction energy for the formation of Li_2O and Li_2O_2 as a function of temperature; b) Ni-based cathode (red) exhibits lower overpotential than the carbon cathode (black) during the first cycle, and the dashed lines are battery operated at 25°C ; c) Raman spectra proves the reversibility of Li_2O at different states; d) online mass spectrometry reveals the Li_2O via four-electron transfer from Li_2O to O_2 during charging; e) the $\text{Li}-\text{O}_2$ cell with molten salt electrolyte based on the Li_2O products could cycle over 150 cycles at 0.2 mA cm^{-2} ; f) operating temperature impacts the composition of cathodic products, Li_2O (red) and Li_2O_2 (yellow). a–f) Reproduced with permission.^[22] Copyright 2018, AAAS. g) Conversion between the Li_2O and $\text{Li}_2\text{O}_2/\text{LiO}_2$ with the potential gap of 0.24 V illustrates the facile redox kinetics of the nanolithia. Reproduced with permission.^[7] Copyright 2016, Springer Nature. h) The schematic shows Li_2O transfer to Li_2O_2 , and the capacity should be limited to 400 mAh g^{-1} to avoid the formation of superoxide and oxygen during the deep charging stage; i) $\text{Li}-\text{Li}_2\text{O}/\text{Ir}/\text{rGO}$ battery can cycle for 2000 times with nearly no capacity loss. h, i) Reproduced with permission.^[108] Copyright 2019, Springer Nature.

electrochemical performance, which seems closer to practical applications than the typical semi-open $\text{Li}-\text{O}_2$ batteries. At the same time, more detailed investigations still need to realize this battery technology.

6. Li_2CO_3

6.1. Li_2CO_3 in $\text{Li}-\text{Air}$ Batteries

Li_2CO_3 (2.80 V vs Li/Li^+) is undesirable side product that will accelerate the premature death of $\text{Li}-\text{air}$ batteries, especially

when operating in the ambient air.^[110] It is usually generated as the result of organic electrolyte decomposition, carbon-based cathode oxidation, and shuttled CO_2 gas contamination.^[111] When Li_2CO_3 formed on the cathode side, its decomposition is troublesome and occurs at higher charging voltage than other products in $\text{Li}-\text{air}$ systems. Ling et al. predicted the decomposition of Li_2CO_3 required a voltage in the range of $4.38\text{--}4.61\text{ V}$ via the first-principles study because it costed higher energy to oxidize the redox-inert anions when Li is extracted.^[69] Undoubtedly, high charge voltage will accelerate the electrode oxidations and electrolyte decompositions, leading to the further accumulation of Li_2CO_3 and, finally, the predeath of the battery.^[112]

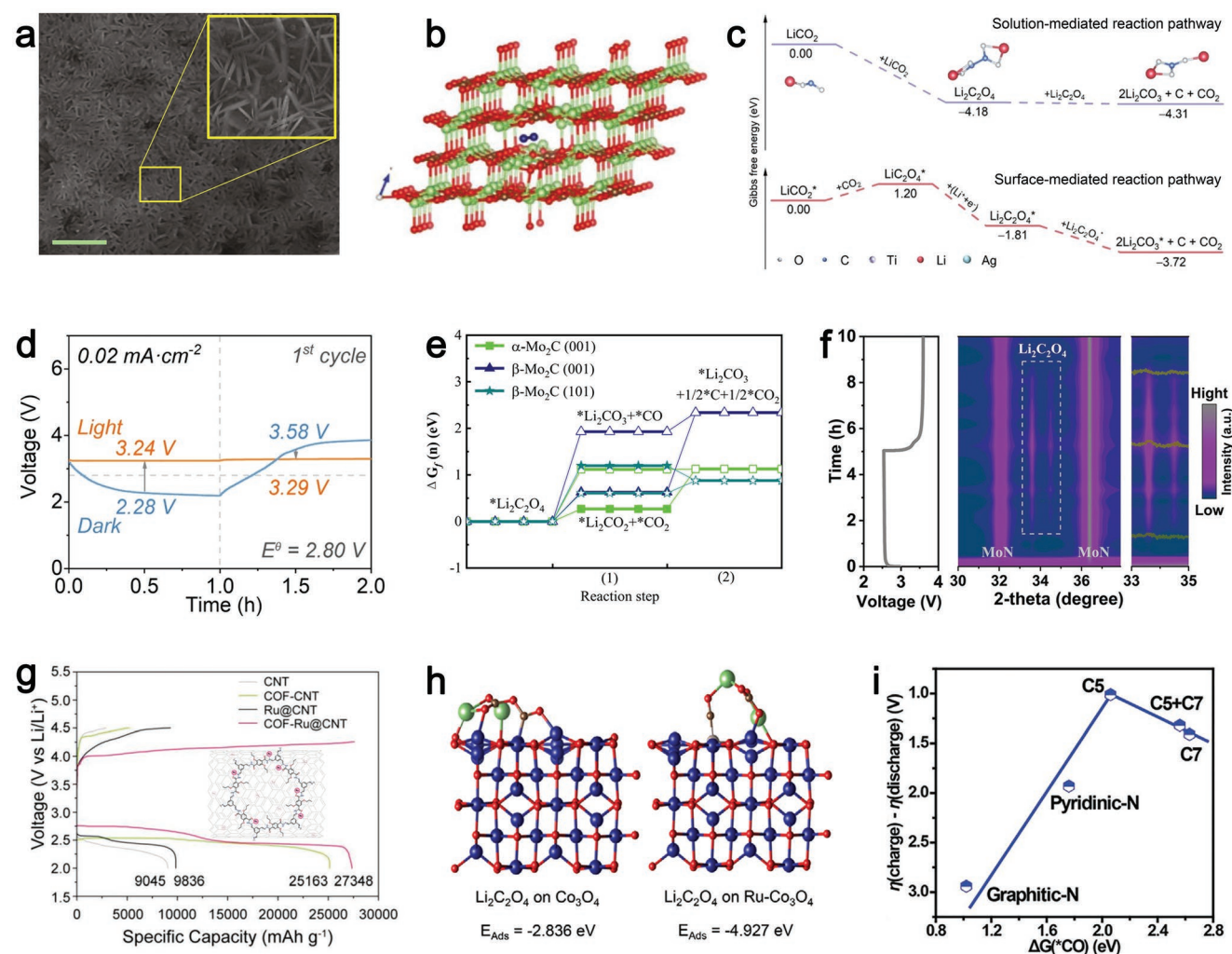


Figure 8. Li_2CO_3 . a) After cycling in the CO_2 atmosphere, Li_2CO_3 forms on the anode; b) the Li_2CO_3 can prevent O_2 transfer to the anode due to the process being endothermic 3.1 eV. a,b) Reproduced with permission.^[110a] Copyright 2018, Springer Nature. c) By comparison of Gibbs free energy diagrams, $\text{Li}-\text{CO}_2$ battery with TNAs@AgNPs cathode forms Li_2CO_3 via solution-mediated reaction pathway, while TNAs cathode via a surface-mediated route. Reproduced with permission.^[117] Copyright 2022, Wiley-VCH. d) $\text{Li}-\text{CO}_2$ batteries with the CNT@ C_3N_4 photocathodes exhibit an ultralow overpotential of 0.04 V. Reproduced with permission.^[118] Copyright 2022, Wiley-VCH. e) $\text{Li}_2\text{C}_2\text{O}_4$ is stable on three kinds of Mo_2C surfaces since the calculated energetic profiles for splitting Li_2CO_3 are endothermic. Reproduced with permission.^[123] Copyright 2020, American Chemical Society. f) $\text{Li}_2\text{C}_2\text{O}_4$ is reversible in battery with MoN nanofibers adhered on carbon cloth (CC@MoN NFs) cathode, as verified by in situ XRD contour plots. Reproduced with permission.^[124] Copyright 2022, Wiley-VCH. g) $\text{Li}-\text{CO}_2$ batteries with covalent organic frameworks and Ru-nanoparticles-decorated CNT (COF-Ru@CNT) cathode display higher capacity and lower overpotential. Reproduced with permission.^[134] Copyright 2019, Wiley-VCH. h) Single-atom Ru on Co_3O_4 has higher adsorption energy for $\text{Li}_2\text{C}_2\text{O}_4$ than Co_3O_4 . Reproduced with permission.^[136] Copyright 2021, Wiley-VCH. i) Overpotential as a function of the adsorption energy of $^*\text{CO}$, in which C5 shows a low theoretical potential gap of 1.01 V. Reproduced with permission.^[137] Copyright 2021, Wiley-VCH.

It is noteworthy that Li_2CO_3 also existed on the lithium anode surface, which could protect the anode from air contamination, including N_2 , CO_2 , and H_2O , thus improving the battery performance in the air atmosphere.^[110] By operating the battery in the CO_2 atmosphere for ten continuous cycles, a $\text{Li}_2\text{CO}_3/\text{C}$ coating was generated on the anode surface (Figure 8a), significantly improving the cycle life of $\text{Li}-\text{air}$ batteries from 11 to 700 times in the simulated air atmosphere. DFT calculations demonstrated that Li_2CO_3 could prevent N_2 and O_2 from migrating to the anode side, while lithium facilely diffused through Li_2CO_3 (Figure 8b).

6.2. Li_2CO_3 in $\text{Li}-\text{CO}_2$ Batteries

At the same time, Li_2CO_3 is the main discharge product in $\text{Li}-\text{CO}_2$ batteries, a new energy storage system that could promote the conversion and utilization of CO_2 .^[113] However, the mechanisms of Li_2CO_3 formation and decomposition are still complicated,^[114] which is related with the CO_2 consumption rate, discharge depth, electrolytes, catalysts, and so on.^[115] Generally, $\text{Li}-\text{CO}_2$ batteries operate via $4\text{Li} + 3\text{CO}_2 \rightleftharpoons 2\text{Li}_2\text{CO}_3 + \text{C}$, 2.80 V, where lithium reacts with CO_2 to generate Li_2CO_3 and carbon species with a balance voltage of 2.80 V.^[116] For the discharge progress, Peng's group calculated the Gibbs free energy of the

Li₂CO₃ formation on the TNAs@AgNPs (Ag nanoparticles electrodeposited on TiO₂ nanotube arrays).^[117] The more negative energy of solution-mediated reaction pathways (−4.31 eV) than that of the surface pathway (−3.72 eV) demonstrated that the former is favorable for the generation of Li₂CO₃ coupled with carbon (Figure 8c).

For the decomposition of Li₂CO₃ in the Li–CO₂ battery, besides the pathway of co-degradation of Li₂CO₃ and carbon species, the theoretical voltage of self-decomposition of Li₂CO₃ is higher (2Li₂CO₃ → 2CO₂ + O₂ + 4Li, 3.82 V). Therefore, during the overall cycling of the CNT@C₃N₄ cathode in the light assistant Li–CO₂ battery, the markedly low charge voltage below 3.82 V, whether in light or dark (Figure 8d), could be attributed to the co-degradation mechanism.^[118] Chen et al. reported that the decomposition of Li₂CO₃ was a multistep reaction.^[119] The Li₂CO₃ was mainly electrochemically decomposed to CO₂ and singlet oxygen ¹O₂ (Li₂CO₃ → 2e[−] + CO₂ + 2Li⁺ + 1/2¹O₂),^[120] followed by the ¹O₂ oxidized carbon substrate and electrolytes to generate CO₂ and CO; in which the carbon cannot react with Li₂CO₃ to release CO₂ via 2Li₂CO₃ + C → 4Li + 3CO₂.

In fact, the electrochemical reaction of Li–CO₂ batteries is very complex, and various discharge products exist.^[121] Yang et al. proposed a different mechanism, lithium oxalate (Li₂C₂O₄, 3.01 V vs Li/Li⁺) is the discharge products for Li–CO₂ batteries with the Mo₂C cathode.^[122] The DFT results indicated that in the presence of Mo₂C catalyst, Li₂C₂O₄ is thermodynamically stable as the final discharge product rather than Li₂CO₃, which was inconsistent with the experimental results.^[123] They attributed this to the disproportionation reactions for splitting Li₂C₂O₄ into Li₂CO₃ need more energy on the Mo₂C surfaces (Figure 8e). Moreover, Cheng et al. also found that the two-electron products Li₂C₂O₄ could reversibly form and decompose on the MoN cathode through experimental and theoretical computation results (Figure 8f).^[124] Similarly, the lithium anode also could react with CO₂ to generate Li₂CO₃ via 2Li + 2CO₂ → Li₂CO₃ + CO,^[23] accompanied by the fuel CO. For example, Wang et al. used 3D porous fractal Zn as the cathode in Li–CO₂ battery, which could produce CO with a faradaic efficiency of 67% by adjusting the discharged current density.^[125] Based on the in situ Raman spectroscopy and DFT calculations, Zhou and colleagues revealed that following the discharge voltage plateau of 2.5 V (4Li⁺ + 3CO₂ + 4e[−] → 2Li₂CO₃ + C, 2.8 V), the new plateau appeared at 1.8 V could be attributed to the 4Li⁺ + CO₂ + 4e[−] → 2Li₂O + C, 1.89 V.^[126] Compared with the gold cathode and Ketjenblack-based porous cathode, the precious metal catalyst Ru could promote the co-oxidization of the generated carbon and Li₂CO₃, realizing the reversible conversion of the Li–CO₂ battery.

In addition to the batteries operating in pure oxygen or carbon dioxide atmosphere, Li–O₂/CO₂ batteries were also developed due to the higher discharge capacity than Li–O₂ batteries.^[127] Introducing CO₂ into pure O₂ makes one step forward to the practical Li–air battery.^[128] The selected solvents^[129] and the prepared cathodes^[130] could significantly influence the discharge products. The main product, Li₂CO₃, may generate/oxidize via diverse models due to the slow kinetics of the CO₂ electrochemical reactions.^[131] Thus, elucidating the complex formation and decomposition mechanism of Li₂CO₃ is crucial for understanding the Li–CO₂ and Li–O₂/CO₂ systems, which is challenging.

6.3. Catalysts for Li₂CO₃

To increase the reaction kinetics of Li₂CO₃ formation and decomposition, various catalysts have been explored in reversible Li–air/CO₂ batteries.^[132] Zhou and co-workers introduced graphene into Li–CO₂ batteries, displaying a high capacity of 14774 mAh g^{−1}.^[133] Loh et al. reported that a covalent organic frameworks cathode with 1D channels (Figure 8g), which were favorable to the diffusion of CO₂ and Li⁺, gave the battery an ultrahigh capacity of 27348 mAh g^{−1} and a low overpotential of 1.24 V.^[134] Liu et al. designed a low-cost transition metal oxide that the NiO nanosheet array accompanied with oxygen vacancies.^[135] The oxygen vacancies could up-shift the d band center and adjust the conductivity, thus optimizing the adsorbability of carbonaceous species and improving the battery's kinetics. In addition, they also prepared a cathode that single-atom Ru atoms implanted onto a Co₃O₄ nanosheet array, in which the Ru site had a more positive charge than the octahedral Co site on Co₃O₄ and an increased binding energy toward the intermediate Li₂C₂O₄ (Figure 8h).^[136] This kind of electron-deficient center could improve the catalytic activity for the CO₂ evolution reaction, which was beneficial to reducing the charging overpotential of the battery. Taking into consideration of the aggregation issues, leaching effects, poor durability of metal-based catalysts, Dai et al. fabricated topological defect-rich graphene as the metal-free cathodes for Li–CO₂ batteries.^[137] It presented good performance, including the discharge capacity, rate capability, high working current density, long-term cycling stability, and low overpotential. The DFT results revealed that the negatively charged carbon atoms in the topological defects could adsorb the positively charged C atoms in CO₂ molecules and intermediates on the catalyst surface. The heterocyclic pentagon ring (C5) showed a low theoretical potential gap of 1.01 V (Figure 8i), exhibiting the high catalytic activity for CO₂ reduction and Li₂CO₃ decomposition. Exploring high-efficient reversible cathode is essential to accelerate the sluggish kinetics of Li₂CO₃ and realize the rechargeability of Li–air/CO₂ batteries.

7. Summary and Outlook

After decades of development, the investigations on discharge products in Li–air batteries have made much progress (Figure 9). The formation and decomposition of discharge products during ORR and OER progress directly determine the battery performance. The discharge products are substantially affected by a combination of factors, such as the test atmosphere, ambient temperature/humidity, the sort of electrolyte, and the cathodic catalyst, which would influence the composition of discharge products and their growth pathway, morphology, and crystallinity. Li₂O₂ is the most common discharge product in aprotic Li–air batteries due to its good stability in the pure oxygen atmosphere; however, its inferior conductivity makes the reported performance of Li₂O₂-based battery still far from the theoretical value. In addition, Li₂O₂ readily reacts with H₂O and CO₂ to further generate LiOH and Li₂CO₃ when the battery is long-term operating in the air atmosphere.^[138] The LiOH and Li₂CO₃ would gradually accumulate at the cathode side, thus decreasing the Li–air batteries'

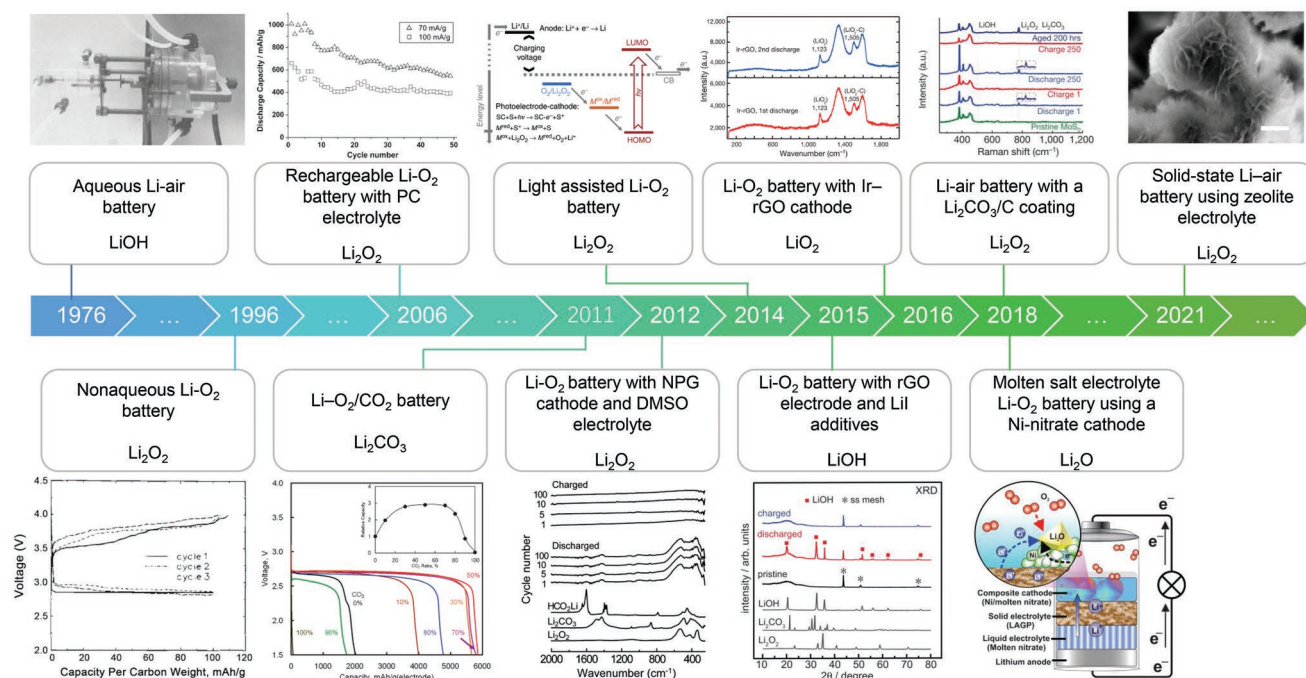


Figure 9. Chronology. Brief timeline for the development of discharge products in Li–air batteries. Image for “Aqueous Li–air batter”: Reproduced with permission.^[12] Copyright 1976, Electrochemical Society, Inc. Image for “Nonaqueous LiO₂ battery”: Reproduced with permission.^[13] Copyright 1996, Electrochemical Society, Inc. Image for “Rechargeable LiO₂ battery with PC electrolyte”: Reproduced with permission.^[14] Copyright 2006, American Chemical Society. Image for LiO₂ battery with NPG cathode and DMSO electrolyte”: Reproduced with permission.^[15c] Copyright 2012, AAAS. Image for “Light-assisted LiO₂ battery”: Image for “LiO₂ battery with rGO electrode and Lil additives”: Reproduced with permission.^[20] Copyright 2015, AAAS. Image for “LiO₂ battery with IrrGO cathode”: Reproduced with permission.^[21] Copyright 2016, Springer Nature. Image for “Reproduced with permission.^[22] Copyright 2018, AAAS. Image for”: Reproduced with permission.^[110a] Copyright 2018, Springer Nature. Image for “LiO₂/CO₂ battery”: Reproduced with permission.^[127] Copyright 2011, The Royal Society of Chemistry. Image for “Solid-state Li-air battery using zeolite electrolyte”: Reproduced with permission.^[154] Copyright 2021, Springer Nature. Image for “Light-assisted Li–O₂ battery”: Reproduced with permission.^[160] Copyright 2014, Springer Nature.

electrochemical behavior and lifespan.^[139] Although LiOH-based Li–air batteries perform exceptionally well, it is challenging to obtain only LiOH as the discharge product, and its growth/decomposition mechanism still needs more exploration. Li₂CO₃ with high stability is relatively difficult to decompose and requires high-efficiency catalysts, especially cycling in the pure CO₂ atmosphere. LiO₂ and Li₂O have been proven reversible but can only stabilize in some specific cases; current research on batteries based on these products is still less, yet they can meet the application of special occasions and thus has the potential for practical application. Encouragingly, many efforts have been devoted to promoting the reversibility of the discharge products, and fundamental understandings have been obtained regarding the Li–air batteries, making the future direction clear. Though the road ahead to the industrialization of Li–air batteries is challenging, we can still reach our objectives with persistent endeavors. During this progress, many vital issues must be addressed.

1. *Mechanisms:* Due to the complexity of Li–air/O₂ systems, the formed crucial discharge products are diverse, such as generally Li₂O₂ in pure oxygen, proton sources promoted LiOH, special catalysts created LiO₂, high-temperature boosted Li₂O, CO₂ supply facilitated Li₂CO₃. Correspondingly, their growth/decomposition pathways are more confused,

especially the Li₂O₂ and Li₂CO₃. It is needed to clarify further the underpinning mechanisms of the redox pathway of the products, reactive intermediates toward solvents, the activity of soluble additives, and undesired by-products, which is conducive to deepening the fundamental understanding of Li–air batteries. Based on these, try to optimize and improve the electrolytes and electrodes to tailor discharge products to give the battery a large discharge capacity, low overpotential, long cycle life, high operating current, and promote their commercial application.

2. *Advanced Technologies:* At present, some in situ characterizations, such as Raman, TEM, and DEMS, have been applied to the Li–air batteries. More leading-edge in situ technologies are required to monitor the products’ dynamic evolution of electronic state, morphology, crystallinity, elemental composition, mass migration, and others. For example, in situ electrochemical TEM could observe the product growth in the liquid electrolyte environment, in situ X-ray absorption spectroscopy could track the average information of products’ bulk particles, cryo-TEM could study the LiO₂ growth pathway on different cathodes,^[99] synchrotron-based XRD could explore the transient changes in the LiOH crystal during battery cycling, operando pressure measurements could confirm discharge products via the number of electrons consumed per mole of gas,^[140] EQCM could reveal the

quantitative information of the deposited products,^[141] X-ray absorption near edge structure analysis could reveal the change in chemical oxidation state and chemical compositions of elements.^[142] In addition, the combination of diverse in situ technologies to monitor the product evolution in one setup could simultaneously achieve more reliable results.

3. **Theoretical Calculations:** The DFT-based theoretical investigation has been widely used in the studies of discharge products in metal–air batteries and fetched much advancement.^[143] It is noteworthy that many limitations still exist in DFT calculations.^[144] The calculated models and parameters in one study may vary from others, leading to results that are difficult to reproduce. The oversimplified systems with just dozens of atoms decreased the computational cost while the accuracy also dropped. Therefore, refining the precise model to simulate the actual working conditions of discharge products is essential to obtain valuable insight into the battery electrochemical reactions. Study the material genome, including ionic radius, crystal structures, conductivity, electronegativity, and so on, to confirm the relationship between battery materials, discharge products, and electrochemical properties and thus screen the potential candidates.^[145] Meanwhile, based on the existing materials database, machine learning and artificial intelligence can be applied to predict the target properties in Li–air batteries, such as molecular properties, chemical reactions, binding energies, and descriptors, to obtain the optimized electrodes and discharge products.^[146]
4. **Promoting Reversibility:** In Li–air batteries, the different atmospheres, electrolytes, catalysts, and other factors can all alter the kind of product. The more severe problem is that, after cycles, the generated products are not single but mixed substances. The complex products seriously impair the Li–air batteries' lifespan and energy efficiency. Therefore, it is highly required stable electrolytes to sustain the highly oxidizing environment and reduce the parasitic products,^[147] effective redox mediators to regulate the OER/ORR progress and increase energy efficiency,^[148] and comprehensive high-efficiency cathodic catalysts to decompose various lithium-containing products and improve reversibility.^[149] In addition, for the metal anode, the corrosion which is always happening during the battery charging and recharging progress should be considered more than the dendrites, whose degradation will increase the serve polarization and thus more irreversible side products. Constructing a protective layer^[110a,150] or developing a metal alloy anode^[151] may be the practical strategy to enhance battery safety and performance.
5. **New Battery Architectures:** With the gradual deepening of research, new types of Li–air/O₂ batteries were proposed, as above-mentioned Li₂O₂-based light-assisted batteries, LiO₂-based sealed batteries, and Li₂O-based high-temperature batteries.^[152] By introducing a superlyophobic membrane, Qiao et al. assembled a hybrid-electrolytes Li–O₂ battery, whose electrolyte was consisted of the aqueous water-in-salt catholyte and nonaqueous ionic liquid anolyte.^[153] Impressively, the discharged product in the water-in-salt electrolyte is Li₂O₂, generated through the proposed solution-based accumulation-hydrolysis mechanism. As a result, the battery with this novel architecture realized a high discharge plateau of 2.85 V, a low overpotential (0.47 V), and a long cycling

lifespan (>250 times) with a limited charging cut-off voltage of 3.6 V. Yu et al. presented a new integrated solid-state Li–air battery based on a lithium-ion-exchanged zeolite X electrolyte.^[154] The discharge products Li₂O₂ displayed a slim nanosheet-like morphology, which is different from the typical toroid. Benefiting from the poor crystallinity of this Li₂O₂, which easily decomposed and thus mitigates the byproducts, the solid-state battery showed much improved electrochemical performance (energy density of 662 Wh kg⁻¹) in ambient air and impressive safety, demonstrating the commercialized potential. It should be noted that solid-state electrolytes with high safety have been widely used in batteries with highly reactive lithium anode.^[155] Advanced solid-state electrolytes with high ionic conductivity and interfacial stability^[156] could accomplish more new Li–air batteries based on different discharge products, bringing more understanding and breakthroughs for the discharge products.^[157]

6. **Specific Application Scenarios:** Currently, Li–air batteries are limited on the lab scale, considering the safety, severe operating conditions, and poor actual performance caused by the low reversibility of discharge products. Therefore, it is tough for the Li–air battery to compete with the commercial Li-ion battery in terms of safety, price, rate performance, stability, cycle life, etc. Developing Li–air batteries based on highly reversible discharge products in the ambient air is highly required and challenging. Applying the batteries in specific scenarios which could tune the formation/decomposition of discharge products is a strategy for their commercialization, such as wide-temperature operation and dry environments. In addition, heightening the strengths of high energy density^[158] and vigorously promoting miniaturized Li–air cells in specific applications,^[159] such as portable power stations, flexible energy storage devices, medical electronics, emergency rescue services, and aerospace exploration, would accelerate this technology forward.

Acknowledgements

This work was supported by Collaborative Research Fund (CRF) (Project no. C5031-20G) of Research Grant Council, University Grants Committee, HK SAR, National Nature Science Foundation of China (22209138), and Guangdong Basic and Applied Basic Research Foundation (2021A1515110464), National Key R&D Program of China (2019YFA0705700), Changchun Science and Technology Development Plan Funding Project (21ZY06), and Youth Innovation Promotion Association CAS (2020230, 2021223).

Conflict of Interest

The authors declare no conflict of interest.

Keywords

discharge products, electrochemical progress, high energy density batteries, Li–air batteries, OER/ORR

Received: September 27, 2022

Revised: December 6, 2022

Published online: March 29, 2023

- [1] L. Zhou, T.-T. Zuo, C. Y. Kwok, S. Y. Kim, A. Assoud, Q. Zhang, J. Janek, L. F. Nazar, *Nat. Energy* **2022**, *7*, 83.
- [2] R. Chen, Q. Li, X. Yu, L. Chen, H. Li, *Chem. Rev.* **2020**, *120*, 6820.
- [3] a) H. Wang, X. Wang, M. Li, L. Zheng, D. Guan, X. Huang, J. Xu, J. Yu, *Adv. Mater.* **2020**, *32*, 2002559; b) S. Zhang, M. Chen, X. Zhao, J. Cai, W. Yan, J. C. Yen, S. Chen, Y. Yu, J. Zhang, *Electrochem. Energy Rev.* **2021**, *4*, 336.
- [4] a) X. Zhang, X. Mu, S. Yang, P. Wang, S. Guo, M. Han, P. He, H. Zhou, *Energy Environ. Mater.* **2018**, *1*, 61; b) D. Aurbach, B. D. McCloskey, L. F. Nazar, P. G. Bruce, *Nat. Energy* **2016**, *1*, 16128; c) Y. Gao, Z. Pan, J. Sun, Z. Liu, J. Wang, *Micro Nano Lett.* **2022**, *14*, 94; d) T. Zhang, N. Wu, Y. Zhao, X. Zhang, J. Wu, J. Weng, S. Li, F. Huo, W. Huang, *Adv. Sci.* **2022**, *9*, 2103954; e) Z. Wu, Y. Tian, H. Chen, L. Wang, S. Qian, T. Wu, S. Zhang, J. Lu, *Chem. Soc. Rev.* **2022**, *51*, 8045.
- [5] W.-J. Kwak, Rosy, D. Sharon, C. Xia, H. Kim, L. R. Johnson, P. G. Bruce, L. F. Nazar, Y.-K. Sun, A. A. Frimer, M. Noked, S. A. Freunberger, D. Aurbach, *Chem. Rev.* **2020**, *120*, 6626.
- [6] K. Chen, D.-Y. Yang, G. Huang, X.-B. Zhang, *Acc. Chem. Res.* **2021**, *54*, 632.
- [7] G. Assat, J.-M. Tarascon, *Nat. Energy* **2018**, *3*, 373.
- [8] a) H.-G. Jung, J. Hassoun, J.-B. Park, Y.-K. Sun, B. Scrosati, *Nat. Chem.* **2012**, *4*, 579; b) Y.-J. Wang, B. Fang, D. Zhang, A. Li, D. P. Wilkinson, A. Ignaszak, L. Zhang, J. Zhang, *Electrochem. Energy Rev.* **2018**, *1*, 1.
- [9] Y. Chen, S. A. Freunberger, Z. Peng, O. Fontaine, P. G. Bruce, *Nat. Chem.* **2013**, *5*, 489.
- [10] J.-H. Kang, J. Lee, J.-W. Jung, J. Park, T. Jang, H.-S. Kim, J.-S. Nam, H. Lim, K. R. Yoon, W.-H. Ryu, I.-D. Kim, H. R. Byon, *ACS Nano* **2020**, *14*, 14549.
- [11] M. M. Ottakam Thotiyil, S. A. Freunberger, Z. Peng, Y. Chen, Z. Liu, P. G. Bruce, *Nat. Mater.* **2013**, *12*, 1050.
- [12] E. L. Littauer, K. C. Tsai, *J. Electrochem. Soc.* **1976**, *123*, 771.
- [13] K. M. Abraham, Z. Jiang, *J. Electrochem. Soc.* **1996**, *143*, 1.
- [14] T. Ogasawara, A. Debart, M. Holzappel, P. Novak, P. G. Bruce, *J. Am. Chem. Soc.* **2006**, *128*, 1390.
- [15] a) A. Débart, A. J. Paterson, J. Bao, P. G. Bruce, *Angew. Chem., Int. Ed.* **2008**, *47*, 4521; b) S. A. Freunberger, Y. Chen, N. E. Drewett, L. J. Hardwick, F. Bardé, P. G. Bruce, *Angew. Chem., Int. Ed.* **2011**, *50*, 8609; c) Z. Peng, S. A. Freunberger, Y. Chen, P. G. Bruce, *Science* **2012**, *337*, 563; d) K. M. Abraham, Z. Jiang, *J. Electrochem. Soc.* **1996**, *143*, 1.
- [16] a) Q. Han, W. Guo, X. He, T. Liu, X. Liu, X. Zhu, T. Bian, L. Jiang, J. Lu, Y. Zhao, *Joule* **2022**, *6*, 381; b) M. Balaish, J. W. Jung, I. D. Kim, Y. Ein-Eli, *Adv. Funct. Mater.* **2019**, *30*, 1808303; c) P. Tan, B. Chen, H. Xu, H. Zhang, W. Cai, M. Ni, M. Liu, Z. Shao, *Energy Environ. Sci.* **2017**, *10*, 2056.
- [17] a) H.-F. Wang, X.-X. Wang, F. Li, J.-J. Xu, *Small Sci.* **2022**, *2*, 2200005; b) T. Liu, Q.-C. Liu, J.-J. Xu, X.-B. Zhang, *Small* **2016**, *12*, 3101.
- [18] a) Q.-C. Liu, J.-J. Xu, S. Yuan, Z.-W. Chang, D. Xu, Y.-B. Yin, L. Li, H.-X. Zhong, Y.-S. Jiang, J.-M. Yan, X.-B. Zhang, *Adv. Mater.* **2015**, *27*, 5241; b) X. Bi, K. Amine, J. Lu, *J. Mater. Chem. A* **2020**, *8*, 3563; c) H. Song, H. Deng, C. Li, N. Feng, P. He, H. Zhou, *Small Methods* **2017**, *1*, 1700135.
- [19] L. Liu, Y. Liu, C. Wang, X. Peng, W. Fang, Y. Hou, J. Wang, J. Ye, Y. Wu, *Small Methods* **2022**, *6*, 2101280.
- [20] T. Liu, M. Leskes, W. Yu, A. J. Moore, L. Zhou, P. M. Bayley, G. Kim, C. P. Grey, *Science* **2015**, *350*, 530.
- [21] J. Lu, Y. J. Lee, X. Luo, K. C. Lau, M. Asadi, H.-H. Wang, S. Brombosz, J. Wen, D. Zhai, Z. Chen, D. J. Miller, Y. S. Jeong, J.-B. Park, Z. Z. Fang, B. Kumar, A. Salehi-Khojin, Y.-K. Sun, L. A. Curtiss, K. Amine, *Nature* **2016**, *529*, 377.
- [22] C. Xia, C. Y. Kwok, L. F. Nazar, *Science* **2018**, *361*, 777.
- [23] S. Xu, S. K. Das, L. A. Archer, *RSC Adv.* **2013**, *3*, 6656.
- [24] a) F. Li, J. Chen, *Adv. Energy Mater.* **2017**, *7*, 1602934; b) K. C. Lau, L. A. Curtiss, J. Greeley, *J. Phys. Chem. C* **2011**, *115*, 23625; c) W. Yang, D. Y. Kim, L. Yang, N. Li, L. Tang, K. Amine, H. K. Mao, *Adv. Sci.* **2017**, *4*, 1600453.
- [25] D. Geng, N. Ding, T. S. A. Hor, S. W. Chien, Z. Liu, D. Wu, X. Sun, Y. Zong, *Adv. Energy Mater.* **2016**, *6*, 1502164.
- [26] Z. Lyu, Y. Zhou, W. Dai, X. Cui, M. Lai, L. Wang, F. Huo, W. Huang, Z. Hu, W. Chen, *Chem. Soc. Rev.* **2017**, *46*, 6046.
- [27] S. Ding, X. Yu, Z.-F. Ma, X. Yuan, *J. Mater. Chem. A* **2021**, *9*, 8160.
- [28] Y. C. Lu, H. A. Gasteiger, E. Crumlin, R. McGuire, Y. Shao-Horn, *J. Electrochem. Soc.* **2010**, *157*, A1016.
- [29] N. B. Aetukuri, B. D. McCloskey, J. M. Garcia, L. E. Krupp, V. Viswanathan, A. C. Luntz, *Nat. Chem.* **2015**, *7*, 50.
- [30] L. Johnson, C. Li, Z. Liu, Y. Chen, S. A. Freunberger, P. C. Ashok, B. B. Praveen, K. Dholakia, J. M. Tarascon, P. G. Bruce, *Nat. Chem.* **2014**, *6*, 1091.
- [31] L. Ma, T. Yu, E. Tzoganakis, K. Amine, T. Wu, Z. Chen, J. Lu, *Adv. Energy Mater.* **2018**, *8*, 1800348.
- [32] D. G. Kwabi, M. Tulodziecki, N. Pour, D. M. Itkis, C. V. Thompson, Y. Shao-Horn, *J. Phys. Chem. Lett.* **2016**, *7*, 1204.
- [33] A. Hu, W. Lv, T. Lei, W. Chen, Y. Hu, C. Shu, X. Wang, L. Xue, J. Huang, X. Du, H. Wang, K. Tang, C. Gong, J. Zhu, W. He, J. Long, J. Xiong, *ACS Nano* **2020**, *14*, 3490.
- [34] J. J. Xu, Z. W. Chang, Y. Wang, D. P. Liu, Y. Zhang, X. B. Zhang, *Adv. Mater.* **2016**, *28*, 9620.
- [35] W. Yao, Y. Yuan, G. Tan, C. Liu, M. Cheng, V. Yurkiv, X. Bi, F. Long, C. R. Friedrich, F. Mashayek, K. Amine, J. Lu, R. Shahbazian-Yassar, *J. Am. Chem. Soc.* **2019**, *141*, 12832.
- [36] Z. Lyu, Y. Zhou, W. Dai, X. Cui, M. Lai, L. Wang, F. Huo, W. Huang, Z. Hu, W. Chen, *Chem. Soc. Rev.* **2017**, *46*, 6046.
- [37] H. K. Lim, H. D. Lim, K. Y. Park, D. H. Seo, H. Gwon, J. Hong, W. A. Goddard, H. Kim, K. Kang, *J. Am. Chem. Soc.* **2013**, *135*, 9733.
- [38] Z. Lyu, L. Yang, Y. Luan, X. Renshaw Wang, L. Wang, Z. Hu, J. Lu, S. Xiao, F. Zhang, X. Wang, F. Huo, W. Huang, Z. Hu, W. Chen, *Nano Energy* **2017**, *36*, 68.
- [39] Y. Li, R. Zhang, B. Chen, N. Wang, J. Sha, L. Ma, D. Zhao, E. Liu, S. Zhu, C. Shi, N. Zhao, *Energy Storage Mater.* **2022**, *44*, 285.
- [40] B. Horstmann, B. Gallant, R. Mitchell, W. G. Bessler, Y. Shao-Horn, M. Z. Bazant, *J. Phys. Chem. Lett.* **2013**, *4*, 4217.
- [41] B. D. Adams, C. Radtke, R. Black, M. L. Trudeau, K. Zaghbi, L. F. Nazar, *Energy Environ. Sci.* **2013**, *6*, 1772.
- [42] S. Lau, L. A. Archer, *Nano Lett.* **2015**, *15*, 5995.
- [43] B. Liu, W. Xu, J. Zheng, P. Yan, E. D. Walter, N. Isern, M. E. Bowden, M. H. Engelhard, S. T. Kim, J. Read, B. D. Adams, X. Li, J. Cho, C. Wang, J.-G. Zhang, *ACS Energy Lett.* **2017**, *2*, 2525.
- [44] J. Li, K. Zhang, B. Wang, H. Peng, *Angew. Chem., Int. Ed.* **2022**, *61*, e202213026.
- [45] M. Li, X. Wang, F. Li, L. Zheng, J. Xu, J. Yu, *Adv. Mater.* **2020**, *32*, 1907098.
- [46] J. S. Hummelshøj, J. Blomqvist, S. Datta, T. Vegge, J. Rossmeisl, K. S. Thygesen, A. C. Luntz, K. W. Jacobsen, J. K. Nørskov, *J. Chem. Phys.* **2010**, *132*, 071101.
- [47] J. Kang, Y. S. Jung, S.-H. Wei, A. C. Dillon, *Phys. Rev. B* **2012**, *85*, 035210.
- [48] Y. F. Mo, S. P. Ong, G. Ceder, *Phys. Rev. B* **2011**, *84*, 205446.
- [49] C. O. Laoire, S. Mukerjee, K. M. Abraham, E. J. Plichta, M. A. Hendrickson, *J. Phys. Chem. C* **2009**, *113*, 20127.
- [50] a) B. D. McCloskey, D. S. Bethune, R. M. Shelby, G. Girishkumar, A. C. Luntz, *J. Phys. Chem. Lett.* **2011**, *2*, 1161; b) S. A. Freunberger, Y. Chen, Z. Peng, J. M. Griffin, L. J. Hardwick, F. Bardé, P. Novák, P. G. Bruce, *J. Am. Chem. Soc.* **2011**, *133*, 8040.
- [51] W. Dai, X. Cui, Y. Zhou, Y. Zhao, L. Wang, L. Peng, W. Chen, *Small Methods* **2019**, *3*, 1800358.
- [52] M. D. Radin, C. W. Monroe, D. J. Siegel, *J. Phys. Chem. Lett.* **2015**, *6*, 3017.

- [53] W. Fan, B. Wang, X. Guo, X. Kong, J. Liu, *Nano Energy* **2016**, *27*, 577.
- [54] Q. Lin, Z. Cui, J. Sun, H. Huo, C. Chen, X. Guo, *ACS Appl. Mater. Interfaces* **2018**, *10*, 18754.
- [55] V. Timoshevskii, Z. Feng, K. H. Bevan, J. Goodenough, K. Zaghib, *Appl. Phys. Lett.* **2013**, *103*, 073901.
- [56] Y. Zhao, C. Ban, J. Kang, S. Santhanagopalan, G.-H. Kim, S.-H. Wei, A. C. Dillon, *Appl. Phys. Lett.* **2012**, *101*, 023903.
- [57] O. Gerbig, R. Merkle, J. Maier, *Adv. Mater.* **2013**, *25*, 3129.
- [58] S. Matsuda, Y. Kubo, K. Uosaki, K. Hashimoto, S. Nakanishi, *J. Phys. Chem. C* **2016**, *120*, 13360.
- [59] H. A. Cortes, V. L. Vildosola, M. A. Barral, H. R. Corti, *Phys. Chem. Chem. Phys.* **2018**, *20*, 16924.
- [60] S. Matsuda, K. Uosaki, S. Nakanishi, *J. Power Sources* **2017**, *353*, 138.
- [61] M. D. Radin, C. W. Monroe, D. J. Siegel, *Chem. Mater.* **2015**, *27*, 839.
- [62] F. Tian, M. D. Radin, D. J. Siegel, *Chem. Mater.* **2014**, *26*, 2952.
- [63] Y. Zhang, Q. Cui, X. Zhang, W. C. Mckee, Y. Xu, S. Ling, H. Li, G. Zhong, Y. Yang, Z. Peng, *Angew. Chem.* **2016**, *128*, 10875.
- [64] R. A. Wong, A. Dutta, C. Yang, K. Yamanaka, T. Ohta, A. Nakao, K. Waki, H. R. Byon, *Chem. Mater.* **2016**, *28*, 8006.
- [65] A. Dutta, R. A. Wong, W. Park, K. Yamanaka, T. Ohta, Y. Jung, H. R. Byon, *Nat. Commun.* **2018**, *9*, 680.
- [66] Y. Yang, W. Liu, N. Wu, X. Wang, T. Zhang, L. Chen, R. Zeng, Y. Wang, J. Lu, L. Fu, L. Xiao, L. Zhuang, *ACS Appl. Mater. Interfaces* **2017**, *9*, 19800.
- [67] a) Z. Guo, X. Dong, S. Yuan, Y. Wang, Y. Xia, *J. Power Sources* **2014**, *264*, 1; b) R. Black, S. H. Oh, J. H. Lee, T. Yim, B. Adams, L. F. Nazar, *J. Am. Chem. Soc.* **2012**, *134*, 2902; c) J. Lei, Z. Gao, L. Tang, L. Zhong, J. Li, Y. Zhang, T. Liu, *Adv. Sci.* **2021**, *9*, 2103760.
- [68] D. G. Kwabi, T. P. Batcho, C. V. Amanchukwu, N. Ortiz-Vitoriano, P. Hammond, C. V. Thompson, Y. Shao-Horn, *J. Phys. Chem. Lett.* **2014**, *5*, 2850.
- [69] C. Ling, R. Zhang, K. Takechi, F. Mizuno, *J. Phys. Chem.* **2014**, *118*, 26591.
- [70] W.-J. Kwak, D. Hirshberg, D. Sharon, H.-J. Shin, M. Afri, J.-B. Park, A. Garsuch, F. F. Chesneau, A. A. Frimer, D. Aurbach, Y.-K. Sun, *J. Mater. Chem. A* **2015**, *3*, 8855.
- [71] Y. Qiao, S. Wu, Y. Sun, S. Guo, J. Yi, P. He, H. Zhou, *ACS Energy Lett.* **2017**, *2*, 1869.
- [72] T. Liu, G. Kim, E. Jónsson, E. Castillo-Martinez, I. Temprano, Y. Shao, J. Carretero-González, R. N. Kerber, C. P. Grey, *ACS Catal.* **2018**, *9*, 66.
- [73] M. Tułodziecki, G. M. Leverick, C. V. Amanchukwu, Y. Katayama, D. G. Kwabi, F. Bardé, P. T. Hammond, Y. Shao-Horn, *Energy Environ. Sci.* **2017**, *10*, 1828.
- [74] C. M. Burke, R. Black, I. R. Kochetkov, V. Giordani, D. Addison, L. F. Nazar, B. D. McCloskey, *ACS Energy Lett.* **2016**, *1*, 747.
- [75] Y. G. Zhu, Q. Liu, Y. Rong, H. Chen, J. Yang, C. Jia, L.-J. Yu, A. Karton, Y. Ren, X. Xu, S. Adams, Q. Wang, *Nat. Commun.* **2017**, *8*, 14308.
- [76] a) G. Leverick, M. Tułodziecki, R. Tatara, F. Bardé, Y. Shao-Horn, *Joule* **2019**, *3*, 1106; b) G. Leverick, Y. G. Zhu, S. Lohmar, F. Bardé, S. Cotte, Y. Shao-Horn, *J. Phys. Chem. C* **2022**, *126*, 8256; c) T. Liu, G. Kim, J. Carretero-González, E. Castillo-Martinez, P. M. Bayley, Z. Liu, C. P. Grey, *Science* **2016**, *352*, 667.
- [77] a) C. L. Bentley, A. M. Bond, A. F. Hollenkamp, P. J. Mahon, J. Zhang, *J. Phys. Chem. C* **2015**, *119*, 22392; b) V. Viswanathan, V. Pande, K. M. Abraham, A. C. Luntz, B. D. McCloskey, D. Addison, *Science* **2016**, *352*, 667.
- [78] M. Carboni, A. G. Marrani, R. Spezia, S. Brutti, *J. Electrochem. Soc.* **2018**, *165*, A118.
- [79] a) J.-B. Park, S. H. Lee, H.-G. Jung, D. Aurbach, Y.-K. Sun, *Adv. Mater.* **2018**, *30*, 1704162; b) X. Bi, M. Li, C. Liu, Y. Yuan, H. Wang, B. Key, R. Wang, R. Shahbazian-Yassar, L. A. Curtiss, J. Lu, K. Amine, *Angew. Chem., Int. Ed.* **2020**, *59*, 22978.
- [80] a) S. Meini, M. Piana, N. Tsiouvaras, A. Garsuch, H. A. Gasteiger, *Electrochem. Solid-State Lett.* **2012**, *15*, A45; b) K. U. Schwenke, M. Metzger, T. Restle, M. Piana, H. A. Gasteiger, *J. Electrochem. Soc.* **2015**, *162*, A573.
- [81] F. Li, S. Wu, D. Li, T. Zhang, P. He, A. Yamada, H. Zhou, *Nat. Commun.* **2015**, *6*, 7843.
- [82] T. Liu, Z. Liu, G. Kim, J. T. Frith, N. Garcia-Araez, C. P. Grey, *Angew. Chem., Int. Ed.* **2017**, *56*, 16057.
- [83] S. Ma, J. Wang, J. Huang, Z. Zhou, Z. Peng, *J. Phys. Chem. Lett.* **2018**, *9*, 3333.
- [84] Q. Xiong, G. Huang, X. B. Zhang, *Angew. Chem., Int. Ed.* **2020**, *59*, 19311.
- [85] A. Dai, Q. Li, T. Liu, K. Amine, J. Lu, *Adv. Mater.* **2019**, *31*, 1805602.
- [86] X. Zhang, P. Dong, J.-I. Lee, J. T. Gray, Y.-H. Cha, S. Ha, M.-K. Song, *Energy Storage Mater.* **2019**, *17*, 167.
- [87] J. Lu, S. Dey, I. Temprano, Y. Jin, C. Xu, Y. Shao, C. P. Grey, *ACS Energy Lett.* **2020**, *5*, 3681.
- [88] J. Wang, S.-J. Kim, J. Liu, Y. Gao, S. Choi, J. Han, H. Shin, S. Jo, J. Kim, F. Ciucci, H. Kim, Q. Li, W. Yang, X. Long, S. Yang, S.-P. Cho, K. H. Chae, M. G. Kim, H. Kim, J. Lim, *Nat. Catal.* **2021**, *4*, 212.
- [89] a) X. Gao, Y. Chen, L. Johnson, P. G. Bruce, *Nat. Mater.* **2016**, *15*, 882; b) X. Lin, Z. Sun, C. Tang, Y. Hong, P. Xu, X. Cui, R. Yuan, Z. Zhou, M. Zheng, Q. Dong, *Adv. Energy Mater.* **2020**, *10*, 2001592; c) Z. Sun, X. Lin, W. Dou, Y. Tan, A. Hu, Q. Hou, R. Yuan, M. Zheng, Q. Dong, *Adv. Energy Mater.* **2022**, *12*, 2102764; d) H. D. Lim, B. Lee, Y. Bae, H. Park, Y. Ko, H. Kim, J. Kim, K. Kang, *Chem. Soc. Rev.* **2017**, *46*, 2873; e) W.-L. Bai, S.-M. Xu, C.-Y. Xu, Q. Zhang, H.-H. Wang, Z. Zhang, X. Chen, S.-Y. Dong, Y.-S. Liu, Z.-X. Xu, X.-G. Zhang, Z. Wang, K.-X. Wang, J.-S. Chen, *J. Mater. Chem. A* **2019**, *7*, 23046.
- [90] a) L. Yang, J. T. Frith, N. Garcia-Araez, J. R. Owen, *Chem. Commun.* **2015**, *51*, 1705; b) S. A. Freunberger, Y. Chen, Z. Peng, J. M. Griffin, L. J. Hardwick, F. Bardé, P. Novák, P. G. Bruce, *J. Am. Chem. Soc.* **2011**, *133*, 8040; c) D. M. Itkis, D. A. Semenenko, E. Y. Kataev, A. I. Belova, V. S. Neudachina, A. P. Sirotnina, M. Hävecker, D. Teschner, A. Knop-Gericke, P. Dudin, A. Barinov, E. A. Goodilin, Y. Shao-Horn, L. V. Yashina, *Nano Lett.* **2013**, *13*, 4697.
- [91] Y.-C. Lu, Y. Shao-Horn, *J. Phys. Chem. Lett.* **2013**, *4*, 93.
- [92] D. Zhai, H.-H. Wang, J. Yang, K. C. Lau, K. Li, K. Amine, L. A. Curtiss, *J. Am. Chem. Soc.* **2013**, *135*, 15364.
- [93] U. Das, K. C. Lau, P. C. Redfern, L. A. Curtiss, *J. Phys. Chem. Lett.* **2014**, *5*, 813.
- [94] M. J. Welland, K. C. Lau, P. C. Redfern, L. Liang, D. Zhai, D. Wolf, L. A. Curtiss, *J. Chem. Phys.* **2015**, *143*, 224113.
- [95] D. Zhai, K. C. Lau, H. H. Wang, J. Wen, D. J. Miller, J. Lu, F. Kang, B. Li, W. Yang, J. Gao, E. Indacochea, L. A. Curtiss, K. Amine, *Nano Lett.* **2015**, *15*, 1041.
- [96] A. Halder, H.-H. Wang, K. C. Lau, R. S. Assary, J. Lu, S. Vajda, K. Amine, L. A. Curtiss, *ACS Energy Lett.* **2018**, *3*, 1105.
- [97] B. Lee, J. Kim, G. Yoon, H.-D. Lim, I.-S. Choi, K. Kang, *Chem. Mater.* **2015**, *27*, 8406.
- [98] L. Luo, B. Liu, S. Song, W. Xu, J. G. Zhang, C. Wang, *Nano-technol.* **2017**, *12*, 535.
- [99] P. Zhang, B. Han, X. Yang, Y. Zou, X. Lu, X. Liu, Y. Zhu, D. Wu, S. Shen, L. Li, Y. Zhao, J. S. Francisco, M. Gu, *J. Am. Chem. Soc.* **2022**, *144*, 2129.
- [100] R. Gao, X. Liang, P. Yin, J. Wang, Y. L. Lee, Z. Hu, X. Liu, *Nano Energy* **2017**, *41*, 535.
- [101] A. Halder, A. T. Ngo, X. Luo, H.-H. Wang, J. G. Wen, P. Abbasi, M. Asadi, C. Zhang, D. Miller, D. Zhang, J. Lu, P. C. Redfern, K. C. Lau, R. Amine, R. S. Assary, Y. J. Lee, A. Salehi-Khojin, S. Vajda, K. Amine, L. A. Curtiss, *J. Phys. Chem. A* **2019**, *123*, 10047.

- [102] S. T. Plunkett, A. Kondori, D. Y. Chung, J. Wen, M. Wolfman, S. H. Lapidus, Y. Ren, R. Amine, K. Amine, A. U. Mane, M. Asadi, S. Al-Hallaj, B. P. Chaplin, K. C. Lau, H.-H. Wang, L. A. Curtiss, *ACS Energy Lett.* **2022**, *7*, 2619.
- [103] L. Chen, J. Yang, Z. Lu, P. Dai, X. Wu, Y. Hong, L. Xiao, L. Huang, H. Bai, S.-G. Sun, *J. Mater. Chem. A* **2022**, *10*, 16570.
- [104] M. D. Radin, J. F. Rodriguez, F. Tian, D. J. Siegel, *J. Am. Chem. Soc.* **2012**, *134*, 1093.
- [105] V. Giordani, D. Tozier, J. Uddin, H. Tan, B. M. Gallant, B. D. McCloskey, J. R. Greer, G. V. Chase, D. Addison, *Nat. Chem.* **2019**, *11*, 1133.
- [106] S.-I. Okuoka, Y. Ogasawara, Y. Suga, M. Hibino, T. Kudo, H. Ono, K. Yonehara, Y. Sumida, Y. Yamada, A. Yamada, M. Oshima, E. Tochigi, N. Shibata, Y. Ikuhara, N. Mizuno, *Sci. Rep.* **2014**, *4*, 5684.
- [107] Z. Zhu, A. Kushima, Z. Y. Yin, L. Qi, K. Amine, J. Lu, J. Li, *Nat. Energy* **2016**, *1*, 16111.
- [108] Y. Qiao, K. Jiang, H. Deng, H. Zhou, *Nat. Catal.* **2019**, *2*, 1035.
- [109] D. Koo, S. J. Kang, *ACS Appl. Mater. Interfaces* **2021**, *13*, 47740.
- [110] a) M. Asadi, B. Sayahpour, P. Abbasi, A. T. Ngo, K. Karis, J. R. Jokisaari, C. Liu, B. Narayanan, M. Gerard, P. Yasaee, X. Hu, A. Mukherjee, K. C. Lau, R. S. Assary, F. Khalili-Araghi, R. F. Klie, L. A. Curtiss, A. Salehi-Khojin, *Nature* **2018**, *555*, 502; b) Z. Zhao, J. Huang, Z. Peng, *Angew. Chem., Int. Ed.* **2018**, *57*, 3874.
- [111] N. Feng, P. He, H. Zhou, *Adv. Energy Mater.* **2016**, *6*, 1502303.
- [112] B. Liu, Y. Sun, L. Liu, J. Chen, B. Yang, S. Xu, X. Yan, *Energy Environ. Sci.* **2019**, *12*, 887.
- [113] a) Z. Xie, X. Zhang, Z. Zhang, Z. Zhou, *Adv. Mater.* **2017**, *29*, 1605891; b) C. Li, Z. Guo, B. Yang, Y. Liu, Y. Wang, Y. Xia, *Angew. Chem., Int. Ed.* **2017**, *56*, 9126; c) X. Hu, Z. Li, J. Chen, *Angew. Chem., Int. Ed. Engl.* **2017**, *56*, 5785.
- [114] Y. Jiao, J. Qin, H. M. K. Sari, D. Li, X. Li, X. Sun, *Energy Storage Mater.* **2021**, *34*, 148.
- [115] X. Mu, H. Pan, P. He, H. Zhou, *Adv. Mater.* **2020**, *32*, 1903790.
- [116] X. Sun, Z. Hou, P. He, H. Zhou, *Energy Fuels* **2021**, *35*, 9165.
- [117] K. Zhang, J. Li, W. Zhai, C. Li, Z. Zhu, X. Kang, M. Liao, L. Ye, T. Kong, C. Wang, Y. Zhao, P. Chen, Y. Gao, B. Wang, H. Peng, *Angew. Chem., Int. Ed.* **2022**, *61*, e202201718.
- [118] J. Li, K. Zhang, Y. Zhao, C. Wang, L. Wang, L. Wang, M. Liao, L. Ye, Y. Zhang, Y. Gao, B. Wang, H. Peng, *Angew. Chem., Int. Ed.* **2022**, *61*, e202114612.
- [119] D. Cao, C. Tan, Y. Chen, *Nat. Commun.* **2022**, *13*, 4908.
- [120] N. Mahne, S. E. Renfrew, B. D. McCloskey, S. A. Freunberger, *Angew. Chem., Int. Ed.* **2018**, *57*, 5529.
- [121] J. Xie, Y. Wang, *Acc. Chem. Res.* **2019**, *52*, 1721.
- [122] C. Yang, K. Guo, D. Yuan, J. Cheng, B. Wang, *J. Am. Chem. Soc.* **2020**, *142*, 6983.
- [123] a) Y. Hou, J. Wang, L. Liu, Y. Liu, S. Chou, D. Shi, H. Liu, Y. Wu, W. Zhang, J. Chen, *Adv. Funct. Mater.* **2017**, *27*, 1700564; b) J. Zhou, X. Li, C. Yang, Y. Li, K. Guo, J. Cheng, D. Yuan, C. Song, J. Lu, B. Wang, *Adv. Mater.* **2019**, *31*, 1804439.
- [124] G. C. Qi, J. X. Zhang, L. Chen, B. Wang, J. L. Cheng, *Adv. Funct. Mater.* **2022**, *32*, 2112501.
- [125] J. Xie, Q. Liu, Y. Huang, M. Wu, Y. Wang, *J. Mater. Chem. A* **2018**, *6*, 13952.
- [126] Y. Qiao, J. Yi, S. Wu, Y. Liu, S. Yang, P. He, H. Zhou, *Joule* **2017**, *1*, 359.
- [127] K. Takechi, T. Shiga, T. Asaoka, *Chem. Commun.* **2011**, *47*, 3463.
- [128] K. Chen, G. Huang, J.-L. Ma, J. Wang, D.-Y. Yang, X.-Y. Yang, Y. Yu, X.-B. Zhang, *Angew. Chem., Int. Ed.* **2020**, *59*, 16661.
- [129] a) H.-K. Lim, H.-D. Lim, K.-Y. Park, D.-H. Seo, H. Gwon, J. Hong, W. A. Goddard, H. Kim, K. Kang, *J. Am. Chem. Soc.* **2013**, *135*, 9733; b) W. Yin, A. Grimaud, F. Lepoivre, C. Yang, J. M. Tarascon, *J. Phys. Chem. Lett.* **2017**, *8*, 214; c) A. Khurram, M. He, B. M. Gallant, *Joule* **2018**, *2*, 2649.
- [130] a) N. Kunanusont, Y. Shimoyama, *ACS Appl. Energy Mater.* **2020**, *3*, 4421; b) Y. Liu, R. Wang, Y. Lyu, H. Li, L. Chen, *Energy Environ. Sci.* **2014**, *7*, 677; c) Y. Qiao, J. Yi, S. Guo, Y. Sun, S. Wu, X. Liu, S. Yang, P. He, H. Zhou, *Energy Environ. Sci.* **2018**, *11*, 1211; d) Q.-C. Zhu, S.-M. Xu, Z.-P. Cai, M. M. Harris, K.-X. Wang, J.-S. Chen, *Energy Storage Mater.* **2017**, *7*, 209.
- [131] E. R. Ezeigwe, L. Dong, R. Manjunatha, Y. Zuo, S.-Q. Deng, M. Tan, W. Yan, J. Zhang, D. P. Wilkinson, *Nano Energy* **2022**, *95*, 106964.
- [132] a) Q. Hao, Z. Zhang, Y. Mao, K. X. Wang, *ChemNanoMat* **2022**, *8*, 202100381; b) J. Li, A. Dai, K. Amine, J. Lu, *Small* **2021**, *17*, 2007760; c) J. Zhou, X. Li, C. Yang, Y. Li, K. Guo, J. Cheng, D. Yuan, C. Song, J. Lu, B. Wang, *Adv. Mater.* **2019**, *31*, 1804439.
- [133] Z. Zhang, Q. Zhang, Y. Chen, J. Bao, X. Zhou, Z. Xie, J. Wei, Z. Zhou, *Angew. Chem., Int. Ed.* **2015**, *54*, 6550.
- [134] X. Li, H. Wang, Z. Chen, H. S. Xu, W. Yu, C. Liu, X. Wang, K. Zhang, K. Xie, K. P. Loh, *Adv. Mater.* **2019**, *31*, 1905879.
- [135] C. Wang, Y. Lu, S. Lu, S. Ma, X. Zhu, Z. Li, Q. Liu, *J. Power Sources* **2021**, *495*, 229782.
- [136] Z. Lian, Y. Lu, C. Wang, X. Zhu, S. Ma, Z. Li, Q. Liu, S. Zang, *Adv. Sci.* **2021**, *8*, 2102550.
- [137] F. Ye, L. Gong, Y. Long, S. N. Talapaneni, L. Zhang, Y. Xiao, D. Liu, C. Hu, L. Dai, *Adv. Energy Mater.* **2021**, *11*, 2101390.
- [138] T. C. M. Nepel, C. G. Anchieta, L. F. Cremasco, B. P. Sousa, A. N. Miranda, L. C. C. B. Oliveira, B. A. B. Francisco, J. P. D. Julio, F. C. B. Maia, R. O. Freitas, C. B. Rodella, R. M. Filho, G. Doubek, *Adv. Energy Mater.* **2021**, *11*, 2101884.
- [139] T. Liu, J. P. Vivek, E. W. Zhao, J. Lei, N. Garcia-Araez, C. P. Grey, *Chem. Rev.* **2020**, *120*, 6558.
- [140] W. Yin, A. Grimaud, F. Lepoivre, C. Yang, J. M. Tarascon, *J. Phys. Chem. Lett.* **2017**, *8*, 214.
- [141] H. Deng, Y. Qiao, X. Zhang, F. Qiu, Z. Chang, P. He, H. Zhou, *J. Mater. Chem. A* **2019**, *7*, 17261.
- [142] a) L. Wang, J. Wang, P. Zuo, *Small Methods* **2018**, *2*, 1700293; b) Q. Sun, J. Liu, B. Xiao, B. Wang, M. Banis, H. Yadegari, K. R. Adair, R. Li, X. Sun, *Adv. Funct. Mater.* **2019**, *29*, 1808332.
- [143] D. Cao, X. Shen, A. Wang, F. Yu, Y. Wu, S. Shi, S. A. Freunberger, Y. Chen, *Nat. Catal.* **2022**, *5*, 193.
- [144] A. Ahmadiparidari, R. E. Warburton, L. Majidi, M. Asadi, A. Chamaani, J. R. Jokisaari, S. Rastegar, Z. Hemmat, B. Sayahpour, R. S. Assary, B. Narayanan, P. Abbasi, P. C. Redfern, A. Ngo, M. Vörös, J. Greeley, R. Klie, L. A. Curtiss, A. Salehi-Khojin, *Adv. Mater.* **2019**, *31*, 1902518.
- [145] a) J. J. de Pablo, N. E. Jackson, M. A. Webb, L.-Q. Chen, J. E. Moore, D. Morgan, R. Jacobs, T. Pollock, D. G. Schlom, E. S. Toberer, J. Analytis, I. Dabo, D. M. DeLongchamp, G. A. Fiete, G. M. Grason, G. Hautier, Y. Mo, K. Rajan, E. J. Reed, E. Rodriguez, V. Stevanovic, J. Suvitvich, K. Thornton, J.-C. Zhao, *npj Comput. Mater.* **2019**, *5*, 41; b) A. O. Boev, S. S. Fedotov, K. J. Stevenson, D. A. Aksyonov, *Comput. Mater. Sci.* **2021**, *197*, 110592.
- [146] a) J.-M. Tarascon, *Nat. Mater.* **2022**, *21*, 979; b) S. Zhai, H. P. Xie, P. Cui, D. Q. Guan, J. Wang, S. Y. Zhao, B. Chen, Y. F. Song, Z. P. Shao, M. Ni, *Nat. Energy* **2022**, *7*, 866.
- [147] J. Zhang, B. Sun, Y. Zhao, A. Tkacheva, Z. Liu, K. Yan, X. Guo, A. M. McDonagh, D. Shanmukaraj, C. Wang, T. Rojo, M. Armand, Z. Peng, G. Wang, *Nat. Commun.* **2019**, *10*, 602.
- [148] a) J. Zhang, B. Sun, Y. Zhao, K. Kretschmer, G. Wang, *Angew. Chem., Int. Ed.* **2017**, *56*, 8505; b) J. Zhang, Y. Zhao, B. Sun, Y. Xie, A. Tkacheva, F. Qiu, P. He, H. Zhou, K. Yan, X. Guo, S. Wang, A. M. McDonagh, Z. Peng, J. Lu, G. Wang, *Sci. Adv.* **2022**, *8*, eabm1899.
- [149] a) Y. Yu, X.-B. Zhang, *Matter* **2019**, *1*, 881; b) N. Cheng, L. Zhang, K. Doyle-Davis, X. Sun, *Electrochem. Energy Rev.* **2019**, *2*, 539.
- [150] T. Liu, X. L. Feng, X. Jin, M. Z. Shao, Y. T. Su, Y. Zhang, X. B. Zhang, *Angew. Chem., Int. Ed.* **2019**, *58*, 18240.

- [151] a) J.-L. Ma, F.-L. Meng, Y. Yu, D.-P. Liu, J.-M. Yan, Y. Zhang, X.-B. Zhang, Q. Jiang, *Nat. Chem.* **2019**, *11*, 64; b) T. Liu, Y. Yu, X.-Y. Yang, J. Wang, X.-B. Zhang, *Small Struct.* **2020**, *1*, 2000015; c) G. Huang, J. Wang, X. Zhang, *ACS Cent. Sci.* **2020**, *6*, 2136.
- [152] Z. Liu, Z. Zhao, W. Zhang, Y. Huang, Y. Liu, D. Wu, L. Wang, S. Chou, *InfoMat* **2022**, *4*, e12260.
- [153] Y. Qiao, Q. Wang, X. Mu, H. Deng, P. He, J. Yu, H. Zhou, *Joule* **2019**, *3*, 2986.
- [154] X. Chi, M. Li, J. Di, P. Bai, L. Song, X. Wang, F. Li, S. Liang, J. Xu, J. Yu, *Nature* **2021**, *592*, 551.
- [155] a) X. Sun, Y. Song, Q. Liu, X. Zhang, H. An, N. Sun, Y. Shi, C. Fu, H. Huo, Y. Xie, Y. Tong, F. Kong, J. Wang, *Sci. Adv.* **2022**, *8*, eabq6261; b) J. Wang, Y. Yin, T. Liu, X. Yang, Z. Chang, X. Zhang, *Nano Res.* **2018**, *11*, 3434.
- [156] a) C. Zhao, Y. Zhu, Q. Sun, C. Wang, J. Luo, X. Lin, X. Yang, Y. Zhao, R. Li, S. Zhao, H. Huang, L. Zhang, S. Lu, M. Gu, X. Sun, *Angew. Chem., Int. Ed.* **2021**, *60*, 5821; b) C. Wang, J. Liang, J. Luo, J. Liu, X. Li, F. Zhao, R. Li, H. Huang, S. Zhao, L. Zhang, J. Wang, X. Sun, *Sci. Adv.* **2021**, *7*, eabh1896; c) P. Tan, H. R. Jiang, X. B. Zhu, L. An, C. Y. Jung, M. C. Wu, L. Shi, W. Shyy, T. S. Zhao, *Appl. Energy* **2017**, *204*, 780.
- [157] M. Kim, H. Lee, H. J. Kwon, S. M. Bak, C. Jaye, D. A. Fischer, G. Yoon, J. O. Park, D. H. Seo, S. B. Ma, D. Im, *Sci. Adv.* **2022**, *8*, eabm8584.
- [158] H. C. Lee, J. O. Park, M. Kim, H. J. Kwon, J.-H. Kim, K. H. Choi, K. Kim, D. Im, *Joule* **2019**, *3*, 542.
- [159] S. Matsuda, M. Ono, S. Yamaguchi, K. Uosaki, *Mater. Horiz.* **2022**, *9*, 856.
- [160] M. Yu, X. Ren, L. Ma, Y. Wu, *Nat. Commun.* **2014**, *5*, 5111.



Tong Liu is a postdoctoral fellow in Prof. Meng Ni's group at the Hong Kong Polytechnic University. He received his Ph.D. degree under the supervision of Prof. Xinbo Zhang at Changchun Institute of Applied Chemistry (CIAC), University of Science and Technology of China. His research interests focus on rechargeable metal–air batteries and electrochemical water-splitting.



Siyuan Zhao received his B.Eng. degree in vehicle engineering from Beijing Institute of Technology in 2020. Now he is a Ph.D. candidate at the Hong Kong Polytechnic University. His research interests focus on metal–air batteries, flexible batteries, and flow batteries.



Meng Ni is a professor and associate dean (Research) at the Faculty of Construction and Environment, The Hong Kong Polytechnic University. He received his Ph.D. degree in mechanical engineering from the University of Hong Kong in 2007. He is a Humboldt Fellow and a Senior Associate editor for *Sustainable Energy Technology and Assessments* (Elsevier) and *e-Prime* (Elsevier) and an Associate editor for the *International Journal of Energy Research* (Wiley), and *International Journal of Green Energy* (Taylor & Francis). His research interests focus on fuel cells, rechargeable metal–air batteries, electrochemical water-splitting, and electrochemical systems for low-grade waste-heat utilization.



Xinbo Zhang is a professor and director of State Key Laboratory of Rare Earth Resource Utilization, Changchun Institute of Applied Chemistry (CIAC), Chinese Academy of Sciences (CAS). He received his Ph.D. degree in Inorganic Chemistry from CIAC and was granted the CAS Presidential Scholarship Award in 2005. Then, during 2005–2010, he worked as a JSPS and NEDO fellow at National Institute of Advanced Industrial Science and Technology (Kansai center), Japan. He has been named Highly Cited Researcher by Clarivate Analytics from 2020 to 2022. His research interests focus on rechargeable batteries and electrocatalysis.